TOWARDS CYBERNETIC MODELING OF BIOLOGICAL PROCESSES IN MAMMALIAN SYSTEMS—LIPID METABOLISM IN THE MURINE MACROPHAGE

by

Lina Aboulmouna

A Dissertation

Submitted to the Faculty of Purdue University

In Partial Fulfillment of the Requirements for the degree of

Doctor of Philosophy

Davidson School of Chemical Engineering

West Lafayette, Indiana

December 2020

THE PURDUE UNIVERSITY GRADUATE SCHOOL
STATEMENT OF COMMITTEE APPROVAL

Dr. Doraiswami Ramkrishna, Chair

The Davidson School of Chemical Engineering

Dr. John Morgan

The Davidson School of Chemical Engineering

Dr. Sangtae Kim

The Davidson School of Chemical Engineering

Dr. Shankar Subramaniam

The University of California, San Diego

Approved by:

Dr. Doraiswami Ramkrishna

Dedicated to the women in my family who have been the backbone of strength and resilience:

my mom Nada and my grandmothers Eelda, Inaam, and Saada

ACKNOWLEDGMENTS

First and foremost, I am grateful for the mentorship, guidance, and support from Professor Doraiswami Ramkrishna (fondly known by many as Ramki). Ramki provided many avenues for me to grow and develop as a scientist and academic through unique opportunities I would not have had under the guidance of any other mentor. More importantly, Ramki encouraged me to ask thoughtful questions and inspired me to think more deeply about the problems I was addressing and critically evaluate my solutions to them. I am grateful for my previous research advisors and predecessors in cybernetic modeling, Dr. Jamey Young (my undergraduate research advisor at Vanderbilt who originally encouraged me to pursue an academic path and continues to serve as a mentor to me) and Dr. Jeff Varner (my graduate advisor at Cornell who played a key role in introducing me to the Ramki Lab at Purdue). Additionally, I am grateful for Professor Arvind Varma for opening the doors for me at Purdue to facilitate my PhD path especially at a time when I was uncertain of my direction.

In addition to my research advisor, Ramki, I am incredibly grateful for the insight and feedback provided by my dissertation committee. In particular, I am grateful for the close mentorship I have received from Dr. Shankar Subramaniam while a visiting scientist in his lab at the University of California, San Diego (UCSD). He generously extended his resources and time in providing his expertise to understanding the biological system studied in this work. I have learned quite a bit about effective science communication and technical writing through his thorough nature. Additionally, Dr. John Morgan provided invaluable insight into my approach to modeling lipid metabolism and extended his own lab resources for my use early on during the start of my time at Purdue when I was transitioning research projects. Dr. Sangtae Kim has provided me with many thought provoking questions that broaden the scope of my work in order to address

pressing scientific questions impacting society at large. I am indebted to my committee members for their guidance and mentorship during the course of my graduate studies.

My colleagues at UCSD Dr. Shakti Gupta and Dr. Mano Maurya both supported me through the early stages of my dissertation work and provided countless hours of feedback regarding my biological system as well as computational expertise. Shakti in particular went above and beyond to support me in excelling and ensured I had the support I needed 24/7. My colleagues at Purdue Dr. Ananth Grama, Dr. Rubesh Raja, Dr. Frank DeVilbiss, and Sana Khanum have provided thoughtful insight into my project as well as been a sounding board for many of my ideas. Additionally, I am indebted to my peers and friends at Vanderbilt, Cornell, Purdue, and UCSD who have supported me through the tumultuous path toward the completion of my PhD. In particular, Akancha Pandey, Dr. Parul Verma, and Dr. Ashley Kaminski who literally supported me in crossing this finish line. Additionally, special thanks to Pelin Bulutoglu, Dr. Shamim Mollah, Dr. Sindhu Raghunandan, Dr. Lara Jazmin, Dr. Tessa Verhoef, and Dr. Gregory Fedorchak.

Finally, I would like to thank my family and friends. My friends have meant a great deal to me throughout the years and have become a part of my larger family. First and foremost, thanks to my mom Nada for her constant support and generosity, my dad Moufid for his support of my academic pursuits, my twin sister Lora for always being there and supporting me through any given scenario without question, my youngest sister Lorina for her thoughtful and inquisitive nature, and my brother Ziad for constantly challenging me both physically and intellectually from a young age. I am grateful to my sister-in-law Amani and the precious gift she is bringing into our family Katarina. A special thanks to my extended family The Aboulmounas and The Kansows, as well as my chosen families: The Froehlichs, The Lowis, The Lunas, The Cowans, Allyson Byrd, Sheena Bhatia, Father Stephen Schumacher, Brooks and Natalie Hollan, Larry and Annie Yatch,

Dr. Jen Esquer, Greg and Ed O'Connor, Jamie Kromm, Emma Fretts, Lauren Mitchell, Julia Litchford, Rayan and Dr. Rima Bouajram, Dr. Rosie Korman, Dr. Martha Ingram, Ananya Sheth, Linda Salgin, Dr. Ashwana Ficker, Kevin Vasquez, Dr. John Foo, Mitesh Patel, Patrick Nash, Alfi Thorsson, Maria Torres-Quevedo, Kenville Hendrickson, Dr. Sampson Lau, Dr. Anne Rocheleau, Dr. Funmi Adebayo, Dr. Casey Garland, Dr. Larissa Wenren, Peg Franken (who has been like a second mom to me), and many more, including my loyal companion and best friend through the years, Buddy.

Last but not least, I would not have been able to complete this milestone and meet all the required deadlines without the constant support of Bev Johnson, Corwin Green, Carol Kling, and Bob Brown, as well as the generous support from the Center for Science of Information (CSoI) staff and funding under grant agreement CCF-0939370. They helped me create a new home at Purdue and UCSD in the midst of what, at times, seemed to be a storm as I navigated the academic waters. They have not only supported me on an academic level throughout my entire graduate career at Purdue, but they have opened doors and opportunities for me that I am forever grateful.

TABLE OF CONTENTS

LIST OF TABLES

LIST OF FIGURES

ABSTRACT

Regulation of metabolism in mammalian cells is achieved through a complex interplay between cellular signaling, metabolic reactions, and transcriptional changes. The modeling of metabolic fluxes in a cell requires the knowledge of all these mechanisms, some of which may be unknown. A cybernetic approach provides a framework to model these complex interactions through the implicit accounting of such regulatory mechanisms, assuming a biological "goal". The goal-oriented control policies of cybernetic models have been used to predict metabolic phenomena ranging from complex substrate uptake patterns and dynamic metabolic flux distributions to the behavior of gene knockout strains. The premise underlying the cybernetic framework is that the regulatory processes affecting metabolism can be mathematically formulated as a cybernetic objective through variables that constrain the network to achieve a specified biological "goal".

Cybernetic theory builds on the perspective that regulation is organized towards achieving goals relevant to an organism's survival or displaying a specific phenotype in response to a stimulus. While cybernetic models have been established by prior work carried out in bacterial systems, we show its applicability to more complex biological systems with a predefined goal. We have modeled eicosanoid, a well-characterized set of inflammatory lipids derived from arachidonic acid, metabolism in mouse bone marrow derived macrophage (BMDM) cells stimulated by Kdo2-Lipid A (KLA, a chemical analogue of Lipopolysaccharide found on the surface of bacterial cells) and adenosine triphosphate (ATP, a danger signal released in response to surrounding cell death) using cybernetic control variables. Here, the cybernetic goal is inflammation; the hallmark of inflammation is the expression of cytokines which act as autocrine signals to stimulate a pro-inflammatory response. Tumor necrosis factor (TNF)-α is an exemplary pro-inflammatory marker

and can be designated as a cybernetic objective for modeling eicosanoid—prostaglandin (PG) and leukotriene (LK)—metabolism. Transcriptomic and lipidomic data for eicosanoid biosynthesis and conversion were obtained from the LIPID Maps database. We show that the cybernetic model captures the complex regulation of PG metabolism and provides a reliable description of PG formation using the treatment ATP stimulation. We then validated our model by predicting an independent data set, the PG response of KLA primed ATP stimulated BMDM cells.

The process of inflammation is mediated by the production of multiple cytokines, chemokines, and lipid mediators each of which contribute to specific individual objectives. For such complex processes in mammalian systems, a cybernetic objective based on a single protein/component may not be sufficient to capture all the biological processes thereby necessitating the use of multiple objectives. The choice of the objective function has been made by intuitive considerations in this thesis. If objectives are conjectured, an argument can be made for numerous alternatives. Since regulatory effects are estimated from unregulated kinetics, one encounters the risk of multiplicity in this regard giving rise to multiple models. The best model is of course that which is able to predict a comprehensive set of perturbations. Here, we have extended our above model to also capture the dynamics of LKs. We have used migration as a biological goal for LK using the chemoattractant CCL2 as a key representative molecule describing cell activation leading to an inflammatory response where a goal composed of multiple cybernetic objectives is warranted. Alternative model objectives included relating both branches of the eicosanoid metabolic network to the inflammatory cytokine TNF-α, as well as the simple maximization of all metabolic products such that each equally contributes to the inflammatory system outcome. We were again able to show that all three cybernetic objectives describing the LK and PG branches for eicosanoid metabolism capture the complex regulation and provide a

reliable description of eicosanoid formation. We performed simulated drug and gene perturbation analyses on the system to identify differences between the models and propose additional experiments to select the best cybernetic model.

The advantage to using cybernetic modeling is in its ability to capture system behavior without the same level of detail required for these interactions as standard kinetic modeling. Given the complexity of mammalian systems, the cybernetic goal for mammalian cells may not be based solely on survival or growth but on specific context dependent cellular responses. In this thesis, we have laid the groundwork for the application of cybernetic modeling in complex mammalian systems through a specific example case of eicosanoid metabolism in BMDM cells, illustrated the case for multiple objectives, and highlighted the extensibility of the cybernetic framework to other complex biological systems.

1 INTRODUCTION

1.1 Mathematical modeling approaches for physiological mechanisms

Engineering methodologies are critical for a quantitative understanding of physiological mechanisms in normal and disease states. The field of systems biology relies upon the use of models to organize biological knowledge and make predictions of complex processes. A variety of multi-omic data and mathematical approaches are available for modeling with varying, simple to complex, degrees of resolution [1, 2]. These models span from the DNA and gene expression levels to intracellular networks, to cell-to-cell and trans-membrane signals, through to the organ level, and even at the multi-cellular organism level. The resulting models can provide greater understanding of the data, identify gaps in our existing knowledge of biological processes, and predict new behaviors that we can explore experimentally. It is critical that we iterate between model and experiments to ensure that our models are realistic and descriptive of the biological phenomena they intend to describe.

One example of metabolic analysis which results in the prediction of dynamics is the reprogramming observed during the diauxie shift in *S. cerevisiae* [3] and requires the integration of kinetics with metabolic regulation and control. Reuss and coworkers have developed structured, un-segregated dynamic models (state averaged over the population) of both *S. cerevisiae* [4] and *E.coli* [5]. These models have been used to simulate the in-vivo dynamics of key pathways such as the Pentose Phosphate Pathway (PPP) and sugar transport in *S. cerevisiae*. Dynamic models of varying complexity have also been constructed to study the penicillin biosynthetic pathway [6], optimized regulatory architectures in metabolic reaction networks [7], red-blood cell metabolic pathways [8], and plant metabolic pathways [9]. However, as demonstrated by cybernetic models

and the complexity of the models from Reuss and coworkers, simultaneously modeling both regulation and reaction kinetics is difficult. The central challenge is uncertainty, both in the parameters as well as the underlying biology. As models continue to grow in complexity, kinetic modeling requires a detailed understanding of reaction mechanisms and regulatory interactions and leads to a rapidly expanding set of adjustable parameters [10]. One approach, cybernetic modeling, has been used for over three decades to predict a variety of metabolic phenomena and incorporates this concept of control without the added burden of typical kinetic frameworks which require detailed knowledge of regulatory mechanisms [11, 12].

1.2 The cybernetic framework

Cybernetic modeling of metabolism, at its core, embodies a framework of ordinary differential equations for kinetic modeling that describes the time-dependent evolution of metabolite concentrations, enzyme concentrations, and cellular growth. In cells, these changes in concentrations, both inside and outside of the cell, are governed by the directed actions of a host of complex biological processes. The cybernetic modeling framework distinguishes itself from traditional kinetic modeling by indirectly accounting for the unknown regulatory processes in the cell. These regulations are a cooperative cascade of molecular mechanisms that enhances a cellular function such as growth or survival. In the absence of high-resolution knowledge of all cellular signaling and metabolic events, cybernetic regulation offers a significant advantage and modulates the level of key enzymes through the introduction of cybernetic variables for induction (u_i) and activation (v_i).

Cybernetic models of metabolism were first formulated to describe the growth behavior of cells in multi-substrate environments. These models build on the assumption that the synthesis and activity of the enzymatic machinery are regulated to maximize a return on investment, such as,

biomass, carbon uptake, etc. [13-15].For example, in the classic scenario of diauxic growth, E. coli regulates its transport enzymes and prioritizes the utilization of the substitutable substrates based on an optimal growth rate [13]. Cybernetic models have been useful in not only describing complex substrate uptake patterns [15] but have also yielded successful predictions of intracellular fluxes [16], gene-knockout behaviors [17], and multiplicity of steady states in chemostats [18]. Since the early abstracted cybernetic models of Dujarti et al. [13] and Kompala et al. [14], which primarily focused upon modeling diauxie growth on mixtures of sugars, cybernetic models have significantly grown in metabolic complexity, albeit not to the degree of the genome scale stoichiometric models. Straight was the first to build an explicit pathway structure into cybernetic models [19], later Ramakrishna et al. [15] built upon this foundation and developed more biologically refined portraits of intracellular networks.

Properly identified cybernetic models can be predictive in many situations because of their goal seeking behavior. The regulation of the genes and the activity of the enzymes are obtained as a solution to an optimal resource allocation problem. However, cybernetic models are complicated and difficult to implement. The work of Varner et al., in particular highlighted both the promise and downside of cybernetic models. A cybernetic model describing 45 genes in the central carbon metabolism of *E.coli* equipped with a description of transcription, translation, and enzyme level regulation was, after model identification on wild-type physiological data, able to predict the physiology of a *pyk* knockout mutant [20]. Optimization of flux through the aspartate amino acid network is another example where a cybernetic model was able to predict the local impact of genetic manipulation (overexpression of feedback resistant pathway enzymes) [21]. Cybernetic models have also been used to study storage product formation and advanced bioreactor control system design [22]. The central issue of model identification is that, in addition to the difficulty in

identifying kinetic parameters, the structure of the optimal control programs governing metabolism must be formulated. Namjoshi and Ramkrishna [23] and later Young and Ramkrishna [24] made significant progress on the cybernetic identification problem.

One strategy that has been proposed to overcome this identification issue is to assume intracellular networks are at a pseudo steady-state. Hybrid cybernetic models (HCM) have addressed shortcomings of the approach by integrating cybernetic optimality concepts with elementary modes (EM; a minimal set of enzymes that can operate at steady state i.e. non-decomposable, non-steady state pathways) [25, 26]. The cybernetic control problem then reduces to a choice between competing steady-state routes through the intracellular network. HCMs dynamically choose combinations of biochemical modes (each catalyzed by a pseudo enzyme whose expression is controlled by an optimal decision) to achieve a physiological objective [25]. This strategy has been applied to model continuous production of lignocellulosic ethanol [27]. Ramkrishna and coworkers extended the HCM concept to lumped HCMs (L-HCM). This approach provides dynamic models for very large networks to be identified with limited data and can be applied to the cybernetic models of the previous generations. Song and Ramkrishna identify ‘‘families’’ of EMs each containing several EMs with one or more unifying characteristics based upon metabolic function [26]. L-HCM can make dynamic predictions with significantly less data due to reduction in parameters and has been applied to an *E.coli* network with 67 reactions and *S.cerevisiae* network with 70 reactions, both of which matched experimental data well [28, 29]. However, their applicability is still constrained by the limitation in the size of the metabolic network that can be used.

To address this limitation, HCM-FBA, developed by Vilkhovoy and Varner, is an alternative approach to HCM, specifically for large networks where the generation of elementary modes is

infeasible. HCM-FBA is a modification of the hybrid approach which uses flux balance analysis (FBA) solutions in conjunction with cybernetic control variables instead of EMs to simulate metabolism. This approach was applied to an aerobic *E. coli* metabolic network that was not feasible with HCM to describe cell mass growth and the shift from glucose to acetate consumption with considerably less modes. The fluxes predicted by HCM-FBA have not yet been validated, and its performance should be compared to lumped hybrid cybernetic models (L-HCM). While cybernetic models have focused on bacterial systems in the past, in this work, we adapt the framework to model the dynamic behavior of prostaglandin (PG) formation as an inflammatory response of bone marrow derived macrophages (BMDM) in a mammalian system [15, 28, 30, 31].

1.3 Cellular regulation

The ability of a cell to process and respond to its surrounding environment and, in turn, adapt in that space is regulated by a complex system of signals that relay information from outside of the cell to its nucleus. Signaling networks are inherently complex and require a systems-level approach to garner insight into the dynamics and connectivity that influence one another. Multiple layers of cellular regulation are required to deconstruct a network and its role within the organism [32]. Cellular signals take on the form of absolute protein levels as well as the location of the protein and interactions among proteins. Furthermore, regulatory factors that influence suppression or promotion of the protein and their corresponding rate, length of time, and relative changes between states is critical to understanding the complexity associated with signaling [30-34].

Protein synthesis and consequently enzyme synthesis require material, energy, and temporal resources. Regarding material and energy resources, protein synthesis requires the presence of a number of cellular components, such as ribosomes, mRNA, tRNA, ATP, and polymerase enzyme

molecules, among others [32,35-36]. Additionally, the time available to produce any one of these cellular components is limited and constrained by the time required by the other activities of the polymerase molecules. The cybernetic framework therefore allows us to propose that the distribution of both material and temporal resources among the available metabolic pathways must be controlled such that the microorganism's survival is optimized [23-27]. The explicit description of even a small fraction of the number of metabolic pathways that compose metabolism is often infeasible. A simpler view of the complexities of reaction networks is required to address these limitations. Otherwise, it would be very difficult to extract any general principles of regulation out of the overwhelming amount of kinetic detail.

1.4 The inflammatory response

Inflammation is an active defense mechanism of multicellular organisms in response to various harmful stressors. The primary role of inflammation is to counter the effects of these stressors and to initiate cell and tissue repair. Multiple factors in the immune system respond to inflammation; for example, macrophages are a type of white blood cell of the immune system designed to target substances which lack surface proteins associated with healthy body cells [32]. Since many inflammatory responses are beneficial, directing and instructing the inflammatory machinery may be a better therapeutic objective than completely suppressing it. This requires the understanding of the biological signaling and regulatory networks, as well as the components involved in the inflammatory response. Macrophages are the key mediators and contributors to the inflammatory response.

1.4.1 Macrophage cells

Macrophages engulf and digest cellular debris, foreign substances, microbes, cancer cells, and anything else that does not have the type of proteins specific to healthy body cells on its surface. Macrophages that promote inflammation are called M1 macrophages, whereas those that decrease inflammation and promote tissue repair are called M2 macrophages. Beyond increasing inflammation and stimulating the immune system, macrophages also play an important anti-inflammatory role and can decrease immune reactions through the release of cytokines.

Macrophages rapidly respond to a stimulus by epigenetic modifications following a cascade of events due to receptor binding. This results in the production of pro-inflammatory cytokines (TNFα, IL-6, IL-12, and type 1 IFN), chemokines, lipid mediators and other anti-microbial molecules. The interaction of the released cytokines, chemokines and lipid mediators with the macrophages and other specific cells in an autocrine and paracrine manner further activate different signaling pathways promoting inflammation through activation of transcription factors like NF-κB and causing the next set of epigenetic modifications leading to expression of specific genes to respond to the infection. Thus, multiple temporal cycles arise. The response by the macrophages are anatomically specific, and so the macrophages of the lung respond differently compared to macrophages of heart. At each step on the cascade, the inflammatory response is regulated.

1.4.2 Response to bacterial infection

Extensive studies have been done to mimic the physiological response of bacterial infection and the inflammatory response on macrophage cells (Figure 1.1) through exposure to the factors lipopolysaccharide (LPS) and adenosine triphosphate (ATP).

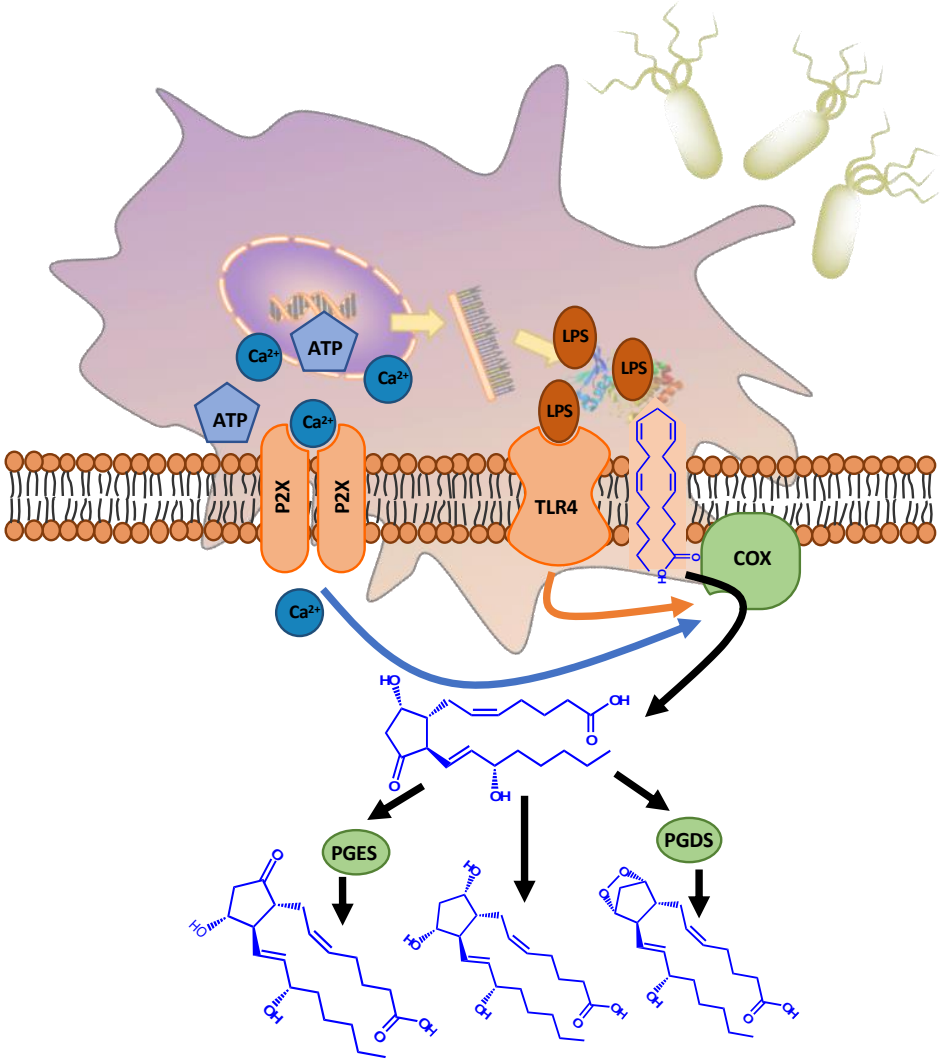

Figure 1.1. Response of a Macrophage to Infection. A simple schematic of a macrophage cell membrane stimulated by lipopolysaccharide (LPS; a structural component in the cell wall of gram-negative bacteria) and adenosine triphosphate (ATP) leads to activation of cyclooxygenase (COX). Arachidonic acid is dislodged from the macrophage cell membrane and then metabolized into prostaglandin products.

1.4.2.1 Lipopolysaccharide

LPS or endotoxin is an integral structural component of the outer cell wall of gram-negative bacteria responsible for the onset of microbial inflammation. LPS stimulates monocytes and

macrophages via toll-like receptors (TLR)-4 which are a type of pattern recognition receptors (Figure 1.1) [33]. The TLR-4 signaling pathway mediates the release of pro- and anti-inflammatory mitogen activated protein kinase cascade nuclear factor kappa-light-chain-enhancer of activated B cells (NFκB) and activator protein (AP)-1 [34]. NFκB is a transcription factor comprised of two subunits represented by either one or two proteins, homo- or hetero-dimers, respectively. Released NFκB migrates into the nuclear space activating transcription of κB-dependent genes such as TNF-α. It is not clear how the TLR-4 receptor becomes activated; however, studies show that LPS binding molecules must be in close proximity to the transmembrane signaling components [35-37]. MD-2 is a non-membrane-spanning molecule that physically associates with TLR-4 and is required for LPS-induced, TLR-4 signaling [38]. It is also not clear on whether or not TLR-4 directly interacts with LPS; however, it is reasonable to assume the role of TLR-4 in cellular response to LPS lies in the initiation of formation of an active signaling complex [39, 40]. MD-2 may change the conformation of the extracellular domain of TLR-4 by changing its affinity to LPS or by functioning as part of a true TLR-4 ligand. Additionally, MD-2 may facilitate oligomerization of activated TLR-4 [35-37].

1.4.2.2 Adenosine triphosphate

The acute release of ATP extracellularly in response to cell stimulation, stress, or tissue damage as well as when extracellular ATP is present at high levels results in a variety of inflammatory responses. It is important to note, ATP can also have an anti-inflammatory response when sustained chronic and low levels of extracellular ATP is released. Some cell types can release ATP through vesicular transport as well as other mechanisms [41]. Examples of this are in the release of ATP through stretch activated channels, voltage dependent anion channels, purinergic receptors involved in opening large pores in the cell membrane, and other channels found to

promote ATP release. Purinergic receptor activation can produce both positive and negative feedback in immune cells to effectively regulate the immune response [42]. Following release of ATP into the cell extracellular space, it is hydrolyzed down to adenosine. This process terminates P2 receptor activation and results in sustained signaling through purinergic receptors. Purinergic receptors which respond to ATP, adenosine, and other similar nucleotides are divided into three major families according to pharmacological and structural features. Specifically, the P2X receptors function as ATP gated ion channels which facilitate influx of extracellular calcium (Ca^{2+}) as well as other cations (Figure 1.1) [43].

1.5 Lipids

The tissue-resident macrophages, upon infection, perform an accessory function of lipid metabolism, in addition to their prototypical roles, such as phagocytosis and destruction of harmful organisms [50,51]. Lipids play a key role in regulating macrophage functions and phenotypes, for example, pathways augmenting β-oxidation and lipid efflux drive immune cells toward an anti-inflammatory phenotype; whereas, pathways facilitating lipid biosynthesis and inflammation favor a pro-inflammatory response. Consequently, we focus our study on the eicosanoids; they are signaling lipids that modulate a diverse set of homeostatic and inflammatory processes linked to various diseases [52]. Eicosanoids arise from the oxidation of Arachidonic acid (AA) by enzymatic pathways: Cyclooxygenase (COX), lipoxygenase (LOX), and cytochrome P450 (CYP450) [53,54]. COXs catalyze the first two biosynthetic steps leading to the production of prostaglandins PGs, i.e., PGE2, PGD2, PGF2α, PGI2 and thromboxane (TXA2). PGs have been found to be responsible for initiating acute inflammation and mediating pain and other symptoms during the inflammatory response [37,53,54]. TXA2 is a pro-inflammatory prostanoid that augments cellular immune responses and has a homeostatic role in platelet aggregation.

Leukotrienes (LTs) and lipoxins (LXs) are 5-LOX derived lipid mediators. LTs exhibit pro-inflammatory action and are produced at the inflammation sites by inflammatory cells. Whereas, LXs are anti-inflammatory as they promote infiltration of monocytes required for resolution and wound healing.

Upon infection, macrophage cells are activated via induced metabolic changes associated with lipids [44, 45]. Lipids have been classified into eight major categories (fatty acyls, glycerolipids, glycerophospholipids, sphingolipids, sterol lipids, prenol lipids, saccharolipids, and polyketides) [46]. Each category of lipids exhibits distinct roles in various cellular processes and disease in addition to cross talk. For example, fatty acyls contribute to inflammation, rheumatoid arthritis, sepsis, and asthma. Consequently, we focus our study on a sub-category of fatty acyls known to contribute to inflammation, the eicosanoids. Eicosanoids are derived from arachidonic acid (AA), a 20-carbon fatty acid, and are further classified into prostaglandins, thromboxanes, leukotrienes, and other oxidized products [47]. PG formation begins when AA is free from its phospholipid bind in the cell membrane. PGs have been found to mediate pain, fever, and other symptoms associated with inflammation [48]. Eicosanoids are synthesized from AA via two pathways: 1) the enzyme Prostaglandin G/H synthase (EC 1.14.99.1; cyclooxygenase (COX)) which has been targeted for treating inflammation, musculoskeletal pain, and other conditions and 2) the enzyme 5-lipoxygenase (LOX) where AA is converted into leukotrienes also known for mediating the inflammatory response.

1.6 Mathematical modeling of lipid metabolism

Eicosanoid metabolism is a complex lipid metabolic network involving the action of numerous signaling molecules, activation of myriad signaling pathways, cells, organs, making modeling the intricate details of the network a challenging task. A systems biology approach

provides a powerful strategy for quantitative understanding of the molecular basis of lipid metabolic networks in mammalian cells by integrating existing mechanistic knowledge and novel high-throughput data. In a growing area of study such as lipid metabolism, descriptive models of system behavior are critical in the understanding of mechanisms, development of therapeutics, and targeting of biomarkers. The integration of mechanistic knowledge and high-throughput data provides a powerful strategy for a quantitative understanding of the molecular basis of the lipid metabolic networks in mammalian cells.

Systems biology allows for the elucidation of novel mechanisms in cellular and molecular machinery. In a growing area of study such as lipid metabolism, descriptive models of system behavior are critical in the understanding of mechanisms, development of therapeutics, and targeting of biomarkers. A systems biology approach provides a powerful strategy for quantitative understanding of the molecular basis of lipid metabolic networks in mammalian cells by integrating existing mechanistic knowledge and novel high-throughput data. Computational simulations enhance our understanding of the biological characteristics of eicosanoid metabolic networks and are critical for the assessment of drug therapeutic effects on elucidating cellular mechanisms.

Eicosanoid metabolism is a complex lipid metabolic network involving the action of numerous signalling molecules, activation of myriad signalling pathways, cells, organs, making modelling the intricate details of the network a challenging task. Systems biology allows for the elucidation of novel mechanisms in cellular and molecular machinery through the integration of mechanistic knowledge and high-throughput data. In a growing area of study such as lipid metabolism in mammalian cells, descriptive models of system behaviour are critical in the understanding of mechanisms, development of therapeutics, and targeting of biomarkers.

Previous research by Gupta et al. developed an approach to model the flux of AA and its downstream metabolites using simple linear kinetics and applied it to data from the murine macrophage-like (RAW 264.7) cells [49]. They also extended this model to bone marrow derived macrophages (BMDM) primed with the lipopolysaccharide (LPS) analogue KDO2-Lipid A (KLA) and activated with a purinergic P2X7 receptor agonist adenosine triphosphate (ATP) [50]. In more recent work, Gupta et al. analyze the effect of $\omega 3$ polyunsaturated fatty acids on normal eicosanoid metabolism in the murine macrophage cell. Their computational model aids in the understanding of competitive metabolism between $\omega 6$ and $\omega 3$ poly unsaturated fatty acids that play a pivotal role in cardiovascular pathologies such as atherosclerosis [51].

1.7 The need for regulation

Lipid biosynthesis often requires the active transport and the chemical transformation of several intermediates. Lipid biosynthesis is further regulated at the corresponding enzyme synthesis levels starting from enzyme transcription through RNA processing, translation, and posttranslational modifications. Lipid mediators regulate the induction and resolution of inflammation; however, increased levels of pro-inflammatory PGs and LTs contribute to a myriad of widespread chronic inflammatory diseases [53,58]. Non-steroidal anti-inflammatory drugs (NSAIDs), one of the most consumed classes of pharmacotherapeutic agents, work by inhibiting the COX-1 and COX-2 pathways [53]. They are beneficial in blocking acute inflammation but are ineffective at terminating inflammation or in promoting resolution and tissue repair. In addition, they also cause side effects, such as gastrointestinal toxicity, mild bleeding side effects, and cardiovascular side effects [53]. These observations motivated researchers to conduct extensive studies on discovering drugs that involve multi-target interventions from a systems biology perspective [59], [60], [61]. Despite their ability to effectively predict metabolite levels, the

existing models either do not incorporate biological regulatory mechanisms or only account for simple regulation such as gene expression level [49-52].

1.8 Research objectives

Simple kinetic models do not capture regulation seen at many stages in cellular function and signaling mechanisms in lipid biosynthesis and often require active transport and the chemical transformation of several intermediates. Lipid biosynthesis is further regulated at the corresponding enzyme synthesis levels starting from enzyme transcription through RNA processing, translation, and post-translational modifications. Despite their ability to effectively predict metabolite levels, the existing models either do not incorporate biological regulatory mechanisms or only account for simple regulation such as gene expression level [38,39,44,45]. Cybernetic models have gone through various evolutions and have shown remarkable success in modeling different biological phenomena in bacterial systems. For complex mammalian cells, cybernetic modeling is in a nascent state and needs refining. Though cybernetic models traditionally followed simplicity, the increase in complexities, due to multiple simultaneous regulations and presence of multiple temporal cycles, warranted the need to incorporate more biological details in the cybernetic objective. Given that biological processes are regulated at many other stages such as posttranslational protein modification or interaction with a protein or substrate molecule, we demonstrate the use of the cybernetic modeling framework to account for such regulation in the modeling of lipid metabolism in a mammalian system in this work.

2 MODELING OF PROSTOGLANDIN METABOLISM

2.1 Summary

The work presented in this section serves to provide a predictive kinetic model incorporating cellular regulatory mechanisms for eicosanoid metabolism and signaling using the cybernetic framework with inflammation as the system objective. While there is no single entity that represents the totality of inflammation by itself, the cytokine tumor necrosis factor alpha (TNF-α) is well-known for its role in the generation of systemic inflammation and is a product of the response of macrophages to ATP and LPS [53, 54]. We hypothesize that PG metabolism is regulated to maximize inflammation characterized by the amount of TNF-α generated by the system. Using the lipid pathways derived from the KEGG pathway database and the time-course data from LIPID MAPS, our cybernetic approach to model the macrophage system provides a quantitative model of eicosanoid metabolism initiated with changes in the levels of AA (input) and resulting in the inflammatory outcome represented by TNF-α [46, 55-58]. The present study is an exemplar that highlights the potential for cybernetic approaches.

2.2 Link between lipids and cytokines

Cytokines are small molecules that function in the signaling (communication) between cells. They can act on other cells through paracrine signaling (close) or endocrine signaling (distant) or even on the cell itself through autocrine signaling. Macrophage cells are a prominent producer of cytokines, specifically in the production of proinflammatory cytokines [59]. Some pro-inflammatory cytokines include IL-1β, IL-6, and TNF-α and are known to be involved in the process of pain. IL-1β specifically is a cytokine released in response to traumatic injury or invasion

and infection by a microbial agent. IL-6 specifically is a cytokine known to appear in response to nerve damage. TNF-α is a well-established cytokine for its role in many pain models [60].

2.3 Methods

To describe the time-dependent formation of PGs, a kinetic model is generated. This description approximates the conversion of AA into intermediate product prostaglandin H2 (PGH_2) and its subsequent conversion into downstream prostaglandin D2 (PGD_2), prostaglandin E2 (PGE_2), and prostaglandin F2α ($PGF_{2\alpha}$). In this simple network of PG formation, the main focus is on how PGH_2 conversion into the three downstream PG products is regulated, which may represent a central decision point in the lipid metabolic system in the macrophage inflammatory response (Figure 2.1.a). The behavior of this network is modeled in three separate conditions: a control, a treatment with ATP, and a combined treatment of ATP and KLA. Measurements were made at 0, 0.25, 0.5, 1, 2, 4, 8, and 20 h after ATP stimulation (Figure 2.1.b). The data for all these conditions was taken from LIPID MAPS [61-64].

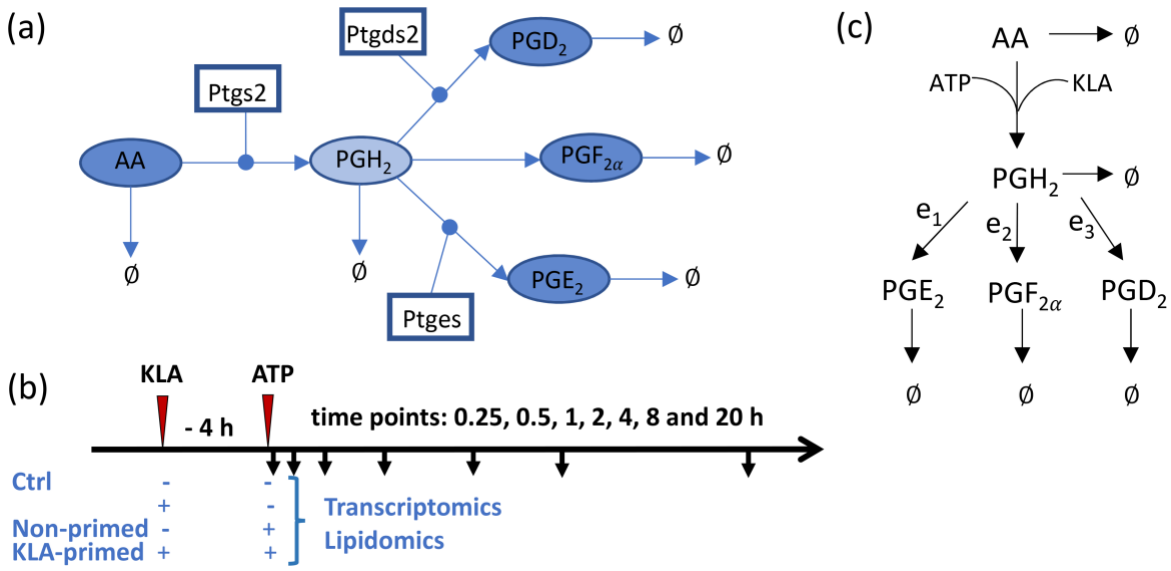

Figure 2.1. Simple Network Map. (a) The arachidonic acid metabolic pathway map for the breakdown of arachidonic acid into respective prostaglandin products via prostaglandin H2 (PGH_2) is shown: (rectangles) enzymes, (ellipses) lipid metabolites, (shaded) measured metabolites, (arrows) enzymatic and non-enzymatic reactions; (b) bone marrow derived macrophages (BMDM) were pretreated with or without KLA for 4 h and then stimulated with or without ATP. The media and cells were collected for lipidomic, tumor necrosis factor alpha (TNF-α) and transcriptomic analysis at 0, 0.25, 0.5, 1, 2, 4, 8, and 20 h after ATP stimulation; (c) depiction of the simplified system network used for kinetic modeling illustrates PGH_2 as a control point and e_1, e_2, and e_3 as cybernetic enzymes regulated via cybernetic variables for the regulation of PGD_2, PGE_2, and $PGF_{2\alpha}$ fluxes.

2.3.1 Development of the kinetic model

The structure of the kinetics for this reaction network is arranged into two segments (Figure 2.1.c). The first describes the conversion of AA into PGH_2 using simple linear kinetics. The kinetics of this reaction is modeled as three separate mechanisms including a basal rate of synthesis, generation due to ATP stimulation, and KLA priming of cells.

$$r_{AA \rightarrow PGH_2} = k_{PGH_2}[AA](1 + k_{ATP}[ATP] + k_{KLA}[KLA]) \quad 2.1$$

To capture the effect of ATP, the treatments to the culture are modeled as a piecewise function, f(t). This piecewise function ramps up to a maximum value of 1 at 0.5 hours (k_s = 2 h^{-1}) and decreases exponentially (k_d = 17.2 h^{-1}) following the initial half hour of the experiment. For KLA, the same f(t) was used with a 4 h adjustment to account for the 4 h priming of KLA prior to ATP stimulation.

$$f(t) = \begin{cases} k_s t & if\ t \leq 0.5 \\ e^{-k_d(t-0.5)} & if\ t > 0.5 \end{cases} \quad 2.2$$

The primary difference in this function from previous work is in the second term which includes exponential decay instead of a linear function to describe desensitization of cells to a given stimulus [65].

2.3.2 The cybernetic framework

The other segment of this model employs the cybernetic framework to capture regulation between the different metabolic options [65]. In the cybernetic framework, there are two descriptions of the reaction kinetics. The first is the raw, enzyme-dependent rate of reaction which we termed the kinetic rate of reaction. This kinetic rate includes an enzyme quantity, e_i, which represents the amount of relative enzyme devoted to the conversion of PGH_2 to a PG product.

$$r^{kin}_{PGH_2 \rightarrow PG_i} = e_i k_{PG_i}[PGH_2] \quad 2.3$$

The second description uses the cybernetic approach which assumes a certain metabolic objective, namely, optimal production of PG derivatives leading to maximum TNF-α production.

The framework views each pathway as a metabolic option to achieve such an objective and describes metabolic regulation in terms of their optimal combinations. Flux through the i^{th} pathway is modeled as regulated by the control of enzyme level and its activity, i.e.,

$$r^{reg}_{PGH_2 \rightarrow PG_i} = v_i r^{kin}_{PGH_2 \rightarrow PG_i} \quad 2.4$$

where, v_i is the cybernetic variable controlling enzyme activity and r^{kin} is the kinetic term. The resulting ordinary differential equations (ODEs) for each metabolite incorporated into the model (Figure 2.1.c) can be written as a combination of regulated rates, r^{reg}, and degradation, where γ is the degradation rate constant, of metabolites:

$$\frac{d[PGH_2]}{dt} = r_{AA \rightarrow PGH_2} - \sum_{i=1} r^{reg}_{PGH_2 \rightarrow PG_i} - \gamma_{PGH_2}[PGH_2] \quad 2.5$$

$$\frac{d[PG_i]}{dt} = r^{reg}_{PGH_2 \rightarrow PG_i} - \gamma_{PG_i}[PG_i] \quad 2.6$$

Enzyme level, e_i, is governed by the following dynamic equations:

$$r^{kin}_{e_i} = k_{e_i}[PGH_2] \quad 2.7$$

$$r^{reg}_{e_i} = u_i r^{kin}_{e_i} \quad 2.8$$

$$\frac{de_{PG_i}}{dt} = \alpha + r^{reg}_{e_i} - \beta e_{PG_i} \quad 2.9$$

where, u_i is the second cybernetic variable regulating the induction of enzyme synthesis, and $r_{e_i}^{kin}$ is the kinetic part of the inducible enzyme synthesis rate. The three terms on the right-hand side denote constitutive, α, and inducible rates of enzyme synthesis modulated by cybernetic variable, u_i, and the decrease of enzyme levels by degradation, defined by β for the rate constant, respectively. The cybernetic control variables, u_i and v_i, are computed from the Matching and Proportional laws, respectively:

$$u_i = \frac{\rho_i}{\sum_k \rho_k} \tag{2.10}$$

$$v_i = \frac{\rho_i}{max_k(\rho_k)} \tag{2.11}$$

where the return-on-investment, ρ_i, is defined by the flux through a particular pathway and is determined based on the designated system goal or objective [24].

2.3.3 Defining the cybernetic goal or objective

PGs are well-characterized for their roles in the inflammatory response. Thus, in this paper, we focus on regulation of PG synthesis as a function of TNF-α, a marker of inflammation, for the selection of the model's objective function. To quantify the relationship between each PG and TNF-α, a simple, linear model of TNF-α production is developed as a function of PG levels:

$$[TNF\alpha] = \sum_i c_i[PG_i] \tag{2.12}$$

We can also approximate the time derivative of TNF-α concentration as a linear combination of time derivatives of PG_i concentrations over the time course. Additionally, due to the difference in magnitude of the different PG_i levels, a scaling was used to determine the contribution of each PG_i pathway leading to TNF-α production. Thus, we define the weights, w_i, as follows:

$$w_i = \frac{c_i\overline{[PG_i]}}{\sum_j c_j\overline{[PG_j]}} \tag{2.13}$$

where w_i (values of 0.2114, 0.2201, and 0.5685 for i = 1, 2, and 3 correspond to PGE_2, $PGF_{2\alpha}$, and PGD_2, respectively) are weights obtained from regression using eight time points across ATP stimulated and control conditions; w_i does not change with time. Of the three pathways modeled, there is a varying degree of inflammation that results from the generation of each PG_i as described by the objective function. In this particular system, the ROI for each pathway is assumed to be the amount of TNF-α that each unregulated pathway can yield at each instant in time which is described by ρ_i.

$$\rho_i = w_i r^{kin}_{PGH_2 \rightarrow PG_i} \tag{2.14}$$

2.3.4 Estimation of the kinetic rate parameters and uncertainty analysis

The model was parameterized using data from two of the three conditions, the control and the ATP treatment cases. Data was available for the AA, PGE_2, $PGF_{2\alpha}$, and PGD_2 metabolites as an 8 point time series over a 20 hour time window. We could not measure the level of PGH_2 because it is an unstable intermediate. Therefore, in the parameter estimation process, we optimized the profile for PGH_2 formation with the constraint that its maximum concentration remains ~10

pmol/μg DNA based on the total amount of PGs produced. The magnitudes of different metabolites varied from 0.001 to 10 pmol/μg of DNA. To fit the model to the data, a least squared fit error was computed from the scaled profiles of the lipid with respect to its maximum value to ensure that the varying magnitude of each PG's level did not skew the parameters towards the sole fit of PGs with higher magnitudes. The overall objective function for fitting the data was to minimize the fit-error between the experimental and the predicted metabolite concentrations [49]:

$$\min_{K,X_o}\left(\sum_{i=1}^{nsp}\left(\sum_{j=1}^{ni}\left(y_{i,j,exp}-y_{i,j,pred}(K,X_0)\right)^2\right)\right) \quad 2.15$$

where K are the parameters or rate constants, X_0 are the initial conditions of enzyme concentrations, ni is the number of time-points, 21, interpolated from 0 to 20 hours (indexed as j) in order to provide equal weightage to later time points in the model fit, and nsp is the total number of species (indexed as i). The ODEs in the model were solved using ode15s for stiff systems in MATLAB (2017, Natick, MA). Parameters (Table 2.1) were optimized using a two-step hybrid optimization procedure that started with a genetic algorithm seeded with random initial parameter values and run up to 100 generations to determine near optimal parameter values (Matlab® function "ga"). The results from the application of the genetic algorithm-based optimization were then further refined using a generalized constrained non-linear optimization employing a gradient search method (Matlab® function "fmincon").

The goodness of the fits was assessed by comparing the variance for the fitted data to the variance in the experimental (replicate) data (treatment and control data combined) using the F-test as follows [50]:

$$F = \frac{SSE_{fit} \Big/ (2 \times nt)}{SSE_{exp} \Big/ (2 \times nt \times (nr - 1))} \quad 2.16$$

$$F = \frac{\left(\sum_{j=1}^{nt} \left(Y_j^{trt} - \bar{X}_j^{trt}\right)^2 + \sum_{j=1}^{nt} \left(Y_j^{ctrl} - \bar{X}_j^{ctrl}\right)^2\right) \Big/ (2 \times nt)}{\left(\sum_{j=1}^{nt} \sum_{i=1}^{nr} \left(X_{ij}^{trt} - \bar{X}_j^{trt}\right)^2 + \sum_{j=1}^{nt} \sum_{i=1}^{nr} \left(X_{ij}^{ctrl} - \bar{X}_j^{ctrl}\right)^2\right) \Big/ (2 \times nt \times (nr - 1))} \quad 2.17$$

where Xj, $\overline{X}$j, and Yj denote the experimental data, mean experimental data, and simulated (fitted) data at time point j, respectively, nr is the number of replicates (nr = 3, indexed as i), nt is the number of time points (nt = 8, indexed as j), and trt and ctrl are treatment and control groups, respectively. The degrees of freedom for determining the F distribution are $df_1 = (2 \times nt)$ and $df_2 = (2 \times nt \times (nr - 1))$. F statistic values smaller than $F_{0.95}$ (16, 32) = 1.97 indicate statistically equal variance in simulated (fitted) and experimental data; whereas, F values smaller than $F_{0.05}$ (16, 32) = 0.4580 indicate the fit-error is statistically smaller than the experimental error.

2.4 Results

2.4.1 Development of the kinetic model for the COX pathway

Our cybernetic model describes the conversion of AA into the intermediate product PGH_2 and its subsequent conversion into downstream prostaglandin products, PGE_2, $PGF_{2\alpha}$, and PGD_2. In this simple network of PG formation, the primary intent is on the regulation of PGH_2 conversion into the three downstream PG products. To address the latter, cybernetic regulation (implementation of u_i and v_i variables) was used at this branch point. The model for the COX

pathway was described by 7 ODEs and 18 kinetic parameters (Table 2.1) in total; these 18 rate constants were estimated using a hybrid optimization approach (Materials and Methods). Using the optimized parameters, the eicosanoid profiles for the control and ATP stimulated case were simulated (Figure 2.2). For most time points, the difference between the simulated and experimental data in both treatment and control conditions fell within the standard error of the mean. The goodness of fit for the model was further examined by performing the F-test, indicating that the fit-error was less than the experimental measurement error (Table 2.2).

Table 2.1. Estimated Reaction Parameters. Reaction parameters were estimated for the eicosanoid metabolism model. The simulated and predicted columns refer to the parameters optimized for ATP stimulated BMDM cells and KLA primed ATP stimulated BMDM cells, respectively. The predicted parameters were further optimized from the simulated parameters within 30% variability.

Parameter	**Simulated**	**Predicted**
k_{pgh2}	0.0022	0.0016
k_{pge2}	0.0044	0.0031
$k_{pgf2\alpha}$	0.0326	0.0339
k_{pgd2}	0.0533	0.0585
γ_{pge2}	0.0062	0.0044
$\gamma_{pgf2\alpha}$	0.0205	0.0197
γ_{pgd2}	0.1275	0.0893
k_{kla}	17.3923	0.0001
k_{atp}	11.9112	8.3379
$k_{E,pge2}$	8.0801	10.4215
$k_{E,pgf2\alpha}$	0.2078	0.1478
$k_{E,pgd2}$	0.2243	0.157
γ_{PGH2}	0.2603	0.3384
α	0.2244	0.2918
β	0.7757	1.0082
$e_{0,pge2}$	0.3974	0.5094
$e_{0,pgf2\alpha}$	0.0133	0.0105
$e_{0,pgd2}$	0.2601	0.3379

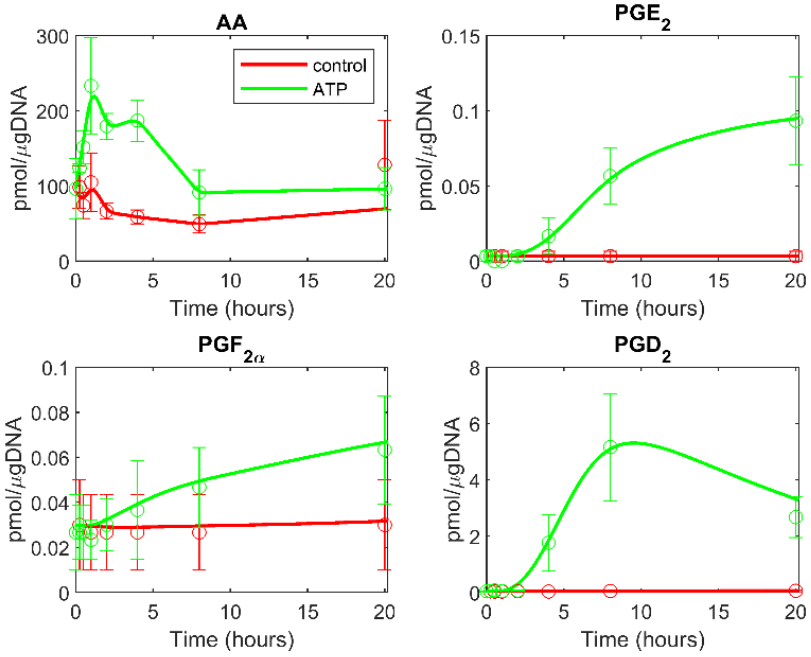

Figure 2.2. Cybernetic Simulation of Eicosanoid Levels. The computational simulation of the eicosanoid profile is generated using the cybernetic model in ATP stimulated BMDM. The mean experimental data (circles) with associated standard error of the mean (SEM) from three replicate experiments (n = 3) for the ATP stimulated (green) and control (red) cases are taken from the mass spectrometry measurements of lipids. The simulation results are shown for the treatment and control cases (solid green and red curves, respectively).

Table 2.2. Model Accuracy. Goodness of fit, F-test, for simulated/optimized (adenosine triphosphate (ATP) stimulated data) and predicted (Kdo2-Lipid A (KLA) primed and ATP stimulated) cases. F values smaller than $F_{0.05}(16, 32) = 0.4580$ indicate that the fit-error is statistically smaller than the experimental error; whereas the F values smaller than $F_{0.95}(16, 32) = 1.97$ indicate that the fit-error is statistically comparable to the experimental error.

Metabolite	**Model Fit to ATP Data**	**Model Fit to KLA and ATP Data**
PGE_2	0.0312	0.2421
$PGF_{2\alpha}$	0.0470	0.0342
PGD_2	0.2636	0.1192

The eicosanoid model robustness was evaluated by performing a parametric sensitivity analysis in which each parameter was varied individually by +/- two-fold of the original optimized value. The slope of each parameter and metabolite sensitivity curve was calculated to evaluate the

sensitivity. A heat map of the slopes was then generated (Figure 2.3). Small to moderate sensitivities in most of the parameters were observed. As expected, very little or no variation in the degradation parameters for PGD_2, PGE_2, and $PGF_{2\alpha}$ or in the KLA parameter is seen in response to metabolite changes. This is especially relevant to note given the data set in which the parameter set was optimized for simulation was not treated with KLA and, consequently, would not have a dependence on this parameter. Based on these results, our model of eicosanoid metabolism is shown to be robust with respect to parametric perturbations.

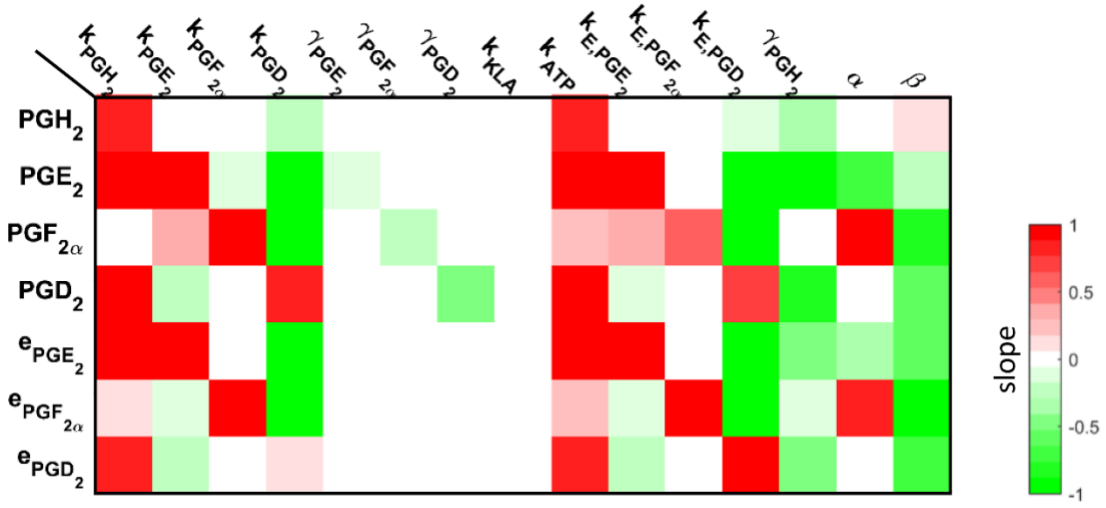

Figure 2.3. Model Robustness. The slope of the sensitivity curves of the arachidonic acid (AA) metabolism are shown as a heat map. For example, the changes in the parameter associated with a conversion of AA into prostaglandin H2 (PGH_2) resulted in an increase in all of the metabolites; whereas, changes in the degradation of PGH_2 resulted in a decrease in all of the metabolites. This is expected, given that PGH_2 is in the upper part of the network, so the changes associated with these parameters will result in an impact on all of the corresponding downstream metabolites.

2.4.2 Prediction of the eicosanoid profile in KLA primed ATP stimulated BMDM

To test the validity of above obtained parameters, we used the parameter values to predict the new data set, the eicosanoid profile in KLA-primed and ATP stimulated BMDM cells. When the profiles were predicted with the optimized parameter values, the model prediction did not fit

the experimental data well. Up to 30% variability was allowed in the optimized parameter values. The range of 30% variability was chosen based on previous work by our group in determining the uncertainty of the calculated parameters in the ATP-stimulated model [50]. The prediction with the relaxed bounds on the parameters yields a good fit to experimental data (Figure 2.4 and see the results of F-test in Table 2.2). This prediction of an independent experimental dataset (KLA primed and ATP stimulated case), which was not used to fit the ATP-stimulation data, further validated the model and parameter values. The mathematical model reflects the AA metabolic network dynamics in BMDM cells.

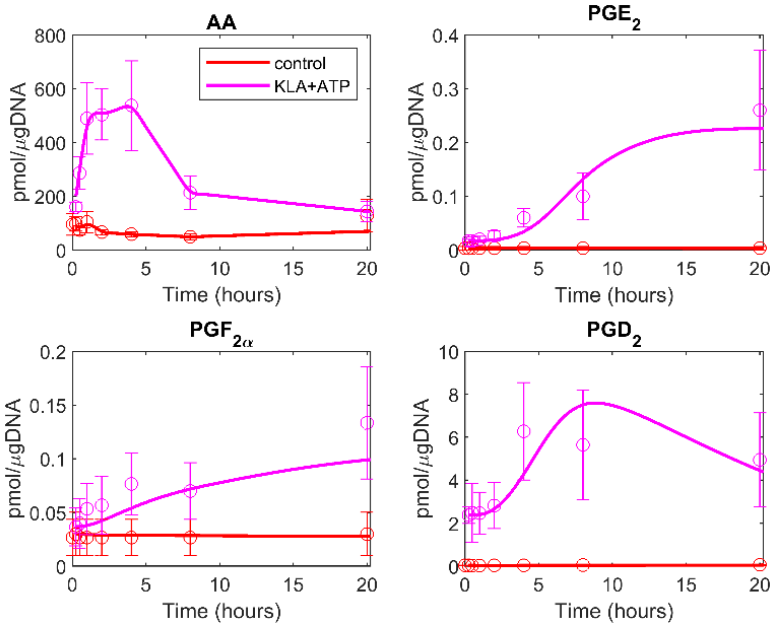

Figure 2.4. Cybernetic Prediction of Eicosanoid Levels. The computational prediction of the eicosanoid profile is generated using the cybernetic model in KLA primed and ATP stimulated BMDM. The mean experimental data (circles) with associated standard error of the mean (SEM) from three replicate experiments (n = 3) for KLA primed ATP-treated (magenta) and control (red) cases are taken from the mass spectrometry measurements of the lipids. The prediction results are shown for the treatment and control cases (solid magenta and red curves, respectively).

2.4.3 Understanding the role of regulation in the cybernetic variables

In order to validate the cybernetic control mechanism that drives the modulation of reaction rates in the model, scaled gene expression data (representative of the enzymes synthesized) were compared to scaled versions of the predicted enzyme levels. The qualitative trends among both the gene expression data and the predicted enzyme levels are expected to be similar [66]. Simply stated, if the gene expression level of the enzyme for one of the pathway branches is increasing over a certain time period, the cybernetic variable for enzyme synthesis control and, therefore, the predicted enzyme levels should also be increasing.

For comparative purposes, we first identified the genes related to the respective branch in the eicosanoid metabolic pathways. These genes were selected using the KEGG database (

Table 2.3) [56, 58]. For two of the three branches in the pathway modeled, there are genes associated with enzymes for the catalysis of those pathways in the network. However, the $PGF_{2\alpha}$ branch is a non-enzymatically regulated process and does not have an associated gene for comparison with the corresponding cybernetic variable.

Table 2.3. Enzyme information. Enzymes were identified from the Kyoto Encyclopedia of Genes and Genomes (KEGG) database and other selected resources for each pathway downstream of prostaglandin H2 (PGH_2) in prostaglandin synthesis. There is not a specific enzyme associated with the regulation of PGH_2 into $PGF_{2\alpha}$.

Entrez ID	Pathway	Gene Symbol	Name
64292	$PGH_2 \rightarrow PGE_2$	Ptges	prostaglandin E synthase
54486	$PGH_2 \rightarrow PGD_2$	Hpgds/Ptgds2	hematopoietic prostaglandin D2 synthase

Gene expression data inform the relative levels of enzyme present. To validate the cybernetic approach, we qualitatively compare gene expression measurements with the corresponding cybernetic enzyme levels. Given gene expression data is represented as a fold change with respect to the control case, we have also taken fold changes of the enzyme levels from the cybernetic model in the treatment cases with respect to their corresponding value in the control cases. Both gene expression and cybernetic enzyme level data was normalized to their corresponding maximum value ($e_i/e_{i,max}$) to visualize a clear comparison of dynamic trends. These comparisons are made for both the ATP and combined KLA primed ATP stimulated treatment conditions. Overall, the scaled predicted enzyme profiles in solid green (ATP stimulated case) and magenta (KLA primed ATP stimulated case) match the general behavior of their corresponding genes identified in

Table 2.3 which are denoted by dashed black lines (Figure 2.5).

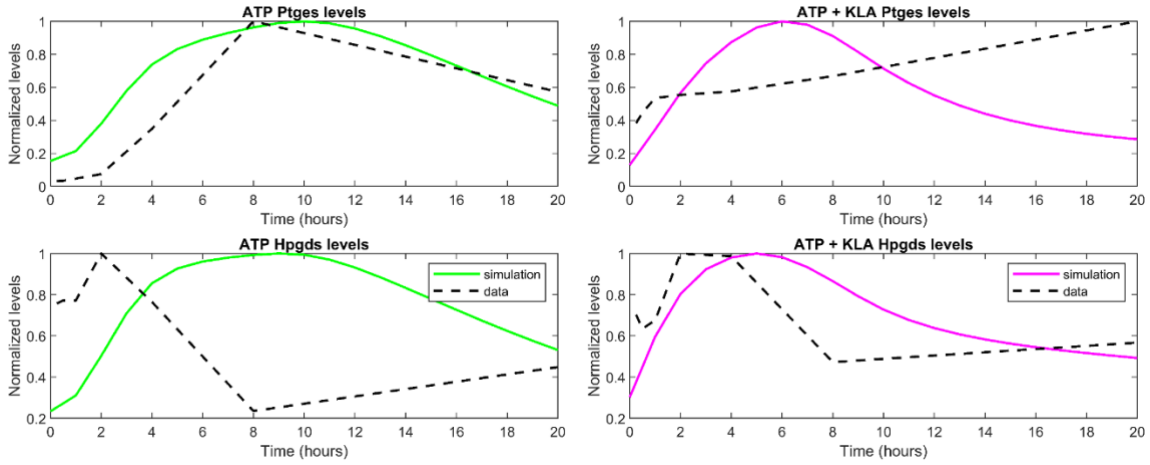

Figure 2.5. The Role of Regulation in the Cybernetic Variables. The behavior of the scaled cybernetic model enzyme level simulations (green in ATP stimulated case and magenta in KLA primed followed by ATP stimulated case) generally match the trends of the scaled gene expression values (black dashed lines) for PtGES and Hpgds/PtGDS2 pathways in (left) ATP and (right) combined KLA primed ATP stimulated treatments.

2.5 Discussion

The cybernetic approach differs substantially from other modeling methods. For traditional kinetic modeling, detailed metabolic regulatory mechanisms are necessary [67, 68]; however, the cybernetic approach models these regulatory actions as a collective process with an optimal system objective. Cybernetic enzymes and variables are used to describe a succinct mode of regulation related to the organism's goal. While we show that cybernetic modeling predicts complex cellular phenomena, we also validate the assumption that the cybernetic control mechanisms mimic cellular regulation [66]. The cybernetic variables for enzyme synthesis and activity, u_i and v_i, are compared with cellular data that is representative of the regulatory mechanisms in cells. We show that the scaled predicted enzyme profiles generally match the behavior of their corresponding genes identified from literature (Section 3.3). These predicted enzyme levels are calculated from metabolomics data and are made on the assumption that enzymes for substrate pathways are regulated in such a way as to optimize the objective function—in this case, formation of TNF-α. The predicted enzyme levels as informed by the e_i control variables are independent of the gene expression data. Qualitatively comparing the behavior of the dynamic gene expression profiles with the predicted enzyme levels further validates our cybernetic model (Figure 2.5) and serves to validate the idea that modeling macrophage cells from a goal-oriented perspective is useful. Additionally, the fact that the model, with the TNF-α objective function, is able to make predictions of the KLA primed and ATP stimulated treatment case, as well as, of gene expression trends validates the use of TNF-α as a control assumption central to the model.

The statistical analysis of multi-omics data coupled with development of mathematical models aid in the unraveling of complex biological systems. In this study, we used a two-step, hybrid optimization approach to estimate rate constants of the AA metabolic network in BMDM

using time-course lipidomic data. All the kinetic parameters in our models were estimated through a nonlinear optimization approach based on the experimental data. Therefore, this study using a multi-omics data-driven systems biology approach is useful for understanding *in vitro* eicosanoid metabolism. Our model showed a good fit to the experimental data as seen from the goodness of fit performed by the F-test (Table 2.2), which suggests that the model captured the key characteristics of the lipid metabolic network in BMDM cells. After fitting parameters to two conditions (i.e., the control and ATP treatment conditions), the model provided the fits which are shown in Figure 2.2. Effectively, this model is reliable as it is also evident that the model correctly explains the evolution of the metabolite concentrations for the different conditions involved in the fit. In the control condition, we see a relatively low rate of prostaglandin formation as we expect. The ATP treatment case shows a good agreement with all prostaglandin products generated, and the kinetics of the model are cross-validated using an additional treatment condition, KLA primed ATP stimulated (Figure 2.4).

We then compared the effective rate constants associated with the enzymes PtGDS2 (EC 5.3.99.2) and PtGES (EC 5.3.99.3) and their corresponding values reported in the literature to confirm the reliability of our optimized parameter values [69-75]. In order to compare the enzyme activities obtained from concentrations in LIPID MAPS experimental data and literature values of enzyme-enriched protein, we used appropriate conversion factors as discussed in Kihara et al., 2014 [50]. In summary, the calculated values from our simulation of eicosanoid metabolism for PtGDS2 activity and PtGES were within the expected range of values reported in the literature. The reported flux of PGD_2 in macrophages is not detectable and determined to be less than 1 nmol/min/mg of total protein which is consistent with our model value, $1x10^{-5}$ nmol/min/mg of total protein [74]. For the flux of PGE_2, the reported literature value of 0.4 pmol/min/mg of total

protein is of the same order as our computed value, 0.1 pmol/min/mg of protein [71]. Our computed values are consistent with those reported in the literature and further validate our computational model.

2.6 Concluding remarks

We have developed a quantitative model of the eicosanoid metabolic pathway by using cybernetic regulation in primary macrophages under control (basal) and ATP stimulation conditions. Additionally, we have been successful in predicting metabolite levels of the eicosanoid profiles and capturing the relative changes in gene expression of relevant enzymes under a set of conditions different from that used for calculating the model rate constants. In particular, we successfully predicted the eicosanoid profiles for the KLA-primed ATP-stimulated case. We have demonstrated the use of the cybernetic approach to model the regulation of mammalian lipid metabolism. The cybernetic model provides a robust description of metabolite formation and can be used to predict perturbations to metabolism. Our computational model assists in understanding the complexity of eicosanoid metabolism and in examining complex regulatory phenomena.

3 MULTI-OBJECTIVES CAPTURE THE DIVERSE BRANCHES OF EICOSANOID FUNCTIONS

3.1 Summary

In general, the cybernetic goal for mammalian cells may not be based solely on survival or growth but on specific context dependent cellular responses. In Chapter 2, we modeled the dynamics of arachidonic acid (AA) metabolism during the inflammatory response of murine bone marrow derived macrophages (BMDM) using a cybernetic approach where the goal of the cell was to defend the organism from infection [86]. Given the complexity of mammalian systems, cells can have multiple biological roles; therefore, the cybernetic goal may be composed of multiple objectives. We show that we are able to effectively capture the dynamics of the eicosanoid network using different cybernetic objectives to describe the system.

3.1.1 The case for multiple objectives

For unicellular organisms, the goal can be as simple as maximizing the organism's growth rate, but for multicellular organisms, the goal may be different and/or more complex depending on the context. For example, the process of inflammation is mediated by the production of multiple cytokines, chemokines, lipid mediators, etc. each of which contribute to specific individual objectives. For complex processes in mammalian systems, a cybernetic objective based on a single protein/component may not be sufficient to capture the biological process thereby necessitating the use of multiple objectives or a single objective dependent on the cellular levels of several biological or molecular components. Below we provide one example of macrophage cell activation leading to an inflammatory response where a goal composed of multiple cybernetic objectives is warranted.

In the case of inflammation, upon binding of lipopolysaccharide (LPS) to the toll like receptor (TLR)-4 on macrophages, signaling pathways such as NF-kB and p38 MAPK pathways are activated, leading to an inflammatory response. This activation results in the production of cytokines, such as TNF-α, interleukin (IL)-2, and IL-10, as well as, upregulation of mRNA for several enzymes involved in production of prostaglandins and other lipids. This activation and upregulation leads to substantial remodeling of lipid metabolism [76-79]. Figure 3.1 illustrates a metabolic network in which various lipids are remodeled during the inflammatory response. This lipid remodeling can be associated with different phenotypes, e.g., eicosanoids, a subcategory of the fatty acyls, are known to contribute to inflammation [61, 80], and ceramides regulate cell survival and apoptosis [81]. From this example, it is clear a single objective may not be able to define the regulation across various lipid categories as a result of multiple functional endpoints.

3.1.2 The eicosanoid oxygenases

Even within eicosanoid metabolism, the cyclooxygenase (COX) enzymes catalyze the production of prostaglandins and thromboxane, while the lipoxygenase (LOX) enzymes catalyze the production of leukotrienes and lipoxins. Prostaglandins are responsible for initiating acute inflammation and mediating pain during the inflammatory response [61, 80, 82]. Thromboxane (TXA2)—a pro-inflammatory prostanoid that augments cellular immune responses and tissue injury—has a homeostatic role in platelet aggregation. Leukotrienes exhibit pro-inflammatory action and are produced at the sites of inflammation. Conversely, lipoxins are anti-inflammatory and promote infiltration of monocytes required for resolution of inflammation and wound healing. The multitude, as well as, variation of signals within the eicosanoid network warrants the use of multiple objectives.

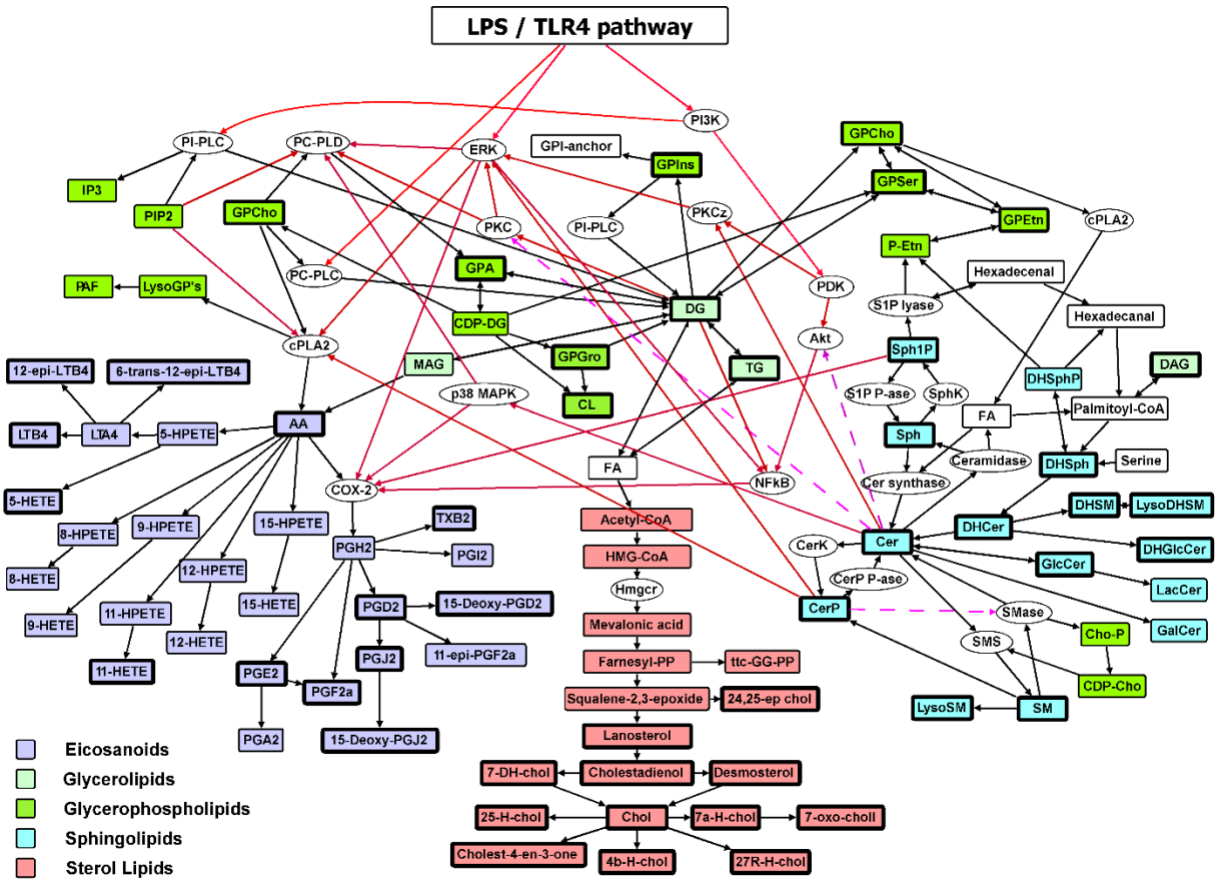

Figure 3.1. Detailed network for LPS-stimulated lipid metabolism and signaling pathway. Black lines represent lipid metabolism, red lines represent signaling pathways, and the magenta dashed lines represent metabolite to protein activity modulations. Metabolites and enzymes are represented in rectangular boxes and oval boxes, respectively. The metabolites are colored based on their lipid categories. The measured and unmeasured metabolites are differentiated by thick and thin borders, respectively [76].

Now, let us consider a single node in the metabolic network, namely the COX2 enzyme. The quantitative level and activity of the COX2 enzyme, linked to AA metabolism, are highly regulated by the activation of NF-κB and p38 MAPK signaling pathways (Figure 3.1). Cells also regulate COX2 by intracellular compartmentation and AA levels [83]. The regulation is, therefore, complex even at a single node in the network. Earlier models have defined enzyme levels using transcriptomic data and incorporated regulation at the transcriptional level only [84, 85]. As

previously discussed in Chapter 2, the cybernetic model by Aboulmouna et al. used a single objective function based on concentrations of TNF-α protein [86]. TNF-α is a key cytokine produced in response to LPS stimulation and has no explicitly known interactions with prostaglandins; however, both the TNF-α and prostaglandin products correlate with increased inflammation. Several other cytokines are also produced during inflammation. TNF-α in combination with other inflammatory cytokines, such as IL-1, IL-6, and IL-12, can serve as a correlate of prostaglandin production [87], however, leukotrienes are known to increase the expression of adhesion proteins and promote cell motility [88]; they can correlate better with chemokines such as CCL2. As a result, each subprocess or even specific node might be correlated with sets of mediator molecules (including cytokines, chemokines, and lipids) pertaining to different objectives.

In the following sections, we explore the use of a single cybernetic objective to describe the network metabolic behavior and compare this to the use of two cybernetic objectives in defining of the system's cybernetic goal.

3.2 Methods

3.2.1 Development of the kinetic model

The structure of the kinetics for this reaction network is again arranged into two segments (Figure 3.2). The first describes the conversion of AA into PGH_2 described by standard linear kinetics and an adapted Michaelis-Menten kinetic equation. The kinetics of this reaction is modeled as three separate mechanisms including a basal rate of synthesis, generation due to ATP stimulation, and KLA priming of cells as follows. The AA is metabolized into n products P_i in the presence of enzyme e_i. For $i = 1$ *to* n,

$$r_{AA\rightarrow P_i} = k_i e_i[AA](1 + k_{atp}[ATP] + k_{kdo}[KDO] + k_{kdoATP}[KDO][ATP]) \quad 3.1$$

The rate of production of P_i from AA can be written as:

$$\frac{dP_i}{dt} = k_i e_i[AA]\left(1 + k_{atp}[ATP] + k_{kdo}[KDO] + k_{kdoATP}[KDO][ATP]\right) - g_i P_i \quad 3.2$$
$$- (downstream\ fluxes)$$

where g_i is the degradation rate constant. Here, Pi represents PGH2, LTA4, 5-HETE, and 15-HETE metabolites in the system (Figure 3.2). It is important to note that PGH2 and LTA4 are unstable intermediates and therefore not measured metabolites in the system (denoted by a translucent circle in Figure 3.2). The enzyme level, e_i, is governed by the following equation:

$$\frac{de_i}{dt} = \alpha + \frac{k_{e,i}[AA]}{[AA] + K_{M,AA}} - \beta e_i \quad 3.3$$

The three terms on the right-hand side denote the constitutive rate α, the maximum inducible rate of enzyme synthesis which takes on the form of Michaelis-Menten kinetics, and the decrease of enzyme level through degradation defined by the rate constant β.

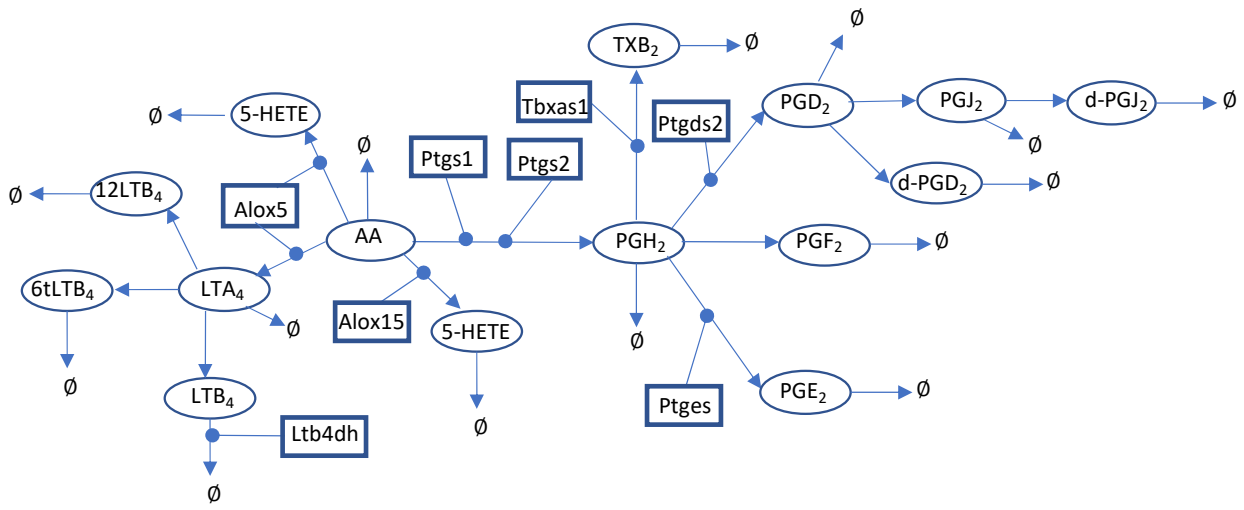

Figure 3.2. Expanded Eicosanoid network of AA metabolism to PG and LK products. The network is divided into 3 sections, AA metabolism, PGH2 metabolism, and LTA4 metabolism.

To capture the effect of ATP and KDO, the treatments to the culture are modeled as a piecewise function

$$f(t) = \begin{cases} k_s t & if\ t \leq 1/k_s \\ \mathrm{e}^{-k_d(t-1/k_s)} & if\ t > k_s \end{cases} \qquad 3.4$$

where kd and ks were determined from a regression model to obtain the piecewise function, f(t). This piecewise function ramps up to a maximum value k_s and the second term which includes exponential decay instead of a linear function to describe desensitization (k_d) of cells to a given stimulus [65].

3.2.2 The cybernetic framework

The other segments of this model employ the cybernetic framework to capture regulation between the different metabolic options [65]. In the cybernetic framework, there are two

descriptions of the reaction kinetics. The first is the raw, enzyme-dependent rate of reaction which we termed the kinetic rate of reaction. This kinetic rate includes an enzyme quantity, e_i, which represents the amount of enzyme e_i devoted to the conversion of substrate metabolite M_s to n product metabolites P_i.

$$M_s \xrightarrow{e_i} P_i \;\; where\; i = 1\; to\; n \tag{3.5}$$

The rate of production of P_i from M_s can be written as:

$$r_{M \to P_i}^{kin} = \; e_i k_{PG_i} [M_s] \tag{3.6}$$

The second description uses the cybernetic approach which assumes a certain metabolic objective, namely, optimal production of PG derivatives leading to maximum TNF-α production. The framework views each pathway as a metabolic option to achieve such an objective and describes metabolic regulation in terms of their optimal combinations. Flux through the i^{th} pathway is modeled as regulated by the control of enzyme level and its activity, i.e.,

$$r_{M_s \to P_i} = r_{P_i}^{kin} v_i \tag{3.7}$$

where $r_{P_i}^{kin}$ is the unregulated rate defined above to produce P_i and v_i is the cybernetic variable controlling enzyme activity. The resulting ordinary differential equations (ODEs) for each metabolite incorporated into the model can be written as a combination of regulated rates

$$\frac{dP_i}{dt} = r_{P_i}^{kin} v_i - g_i P_i \tag{3.8}$$

where g_i is the degradation rate constant. The enzyme level, e_i, is governed by the following equation:

$$r_{e_i}^{kin} = k_{e_i}[M_s] \tag{3.9}$$

$$\frac{de_i}{dt} = \alpha + r_{e_i}^{kin} u_i - \beta e_i \tag{3.10}$$

where u_i is the cybernetic variable regulating the rate of enzyme synthesis. The three terms on the right-hand side denote the constitutive rate α, the maximum inducible rate $r_{e_i}^{kin}$ of enzyme synthesis modulated by cybernetic variable u_i, and the decrease of enzyme level through degradation defined by the rate constant β.

The cybernetic control variables, u_i and v_i, are computed from the Matching and Proportional laws, respectively:

$$u_i = \frac{\rho_i}{\sum_k \rho_k} \tag{3.11}$$

$$v_i = \frac{\rho_i}{max_k(\rho_k)} \tag{3.12}$$

where the return-on-investment, ρ_i, is defined by the flux through a particular pathway and is determined based on the designated system goal or objective [24].

3.2.3 Defining the cybernetic objective

PGs are well-characterized for their roles in the inflammatory response. Thus, in Chapter 2 (Aboulmouna et al), we focused on regulation of PG synthesis as a function of TNF-α, a marker of inflammation, for the selection of the model's objective function. However, we explore the possibility of a combined objective for the approach of modeling the expanded network. To quantify the relationship between metabolites and the designated cytokine for each corresponding branch of the network a simple, linear ODE for the rate of cytokine (e.g., TNF-α) is developed as a function of metabolite m_i (e.g., PGE_2) levels:

$$\frac{d[C_j]}{dt} = \sum_i h_i[m_i] - \gamma[C_j] \tag{3.13}$$

We can also approximate the time derivative of TNF-α concentration as a linear combination of time derivatives of PG_i concentrations over the time course. To determine the contribution of each m_i pathway leading to TNF-α production we define the weights, w_i, as follows:

$$w_i = \frac{h_i}{\sum_j h_j} \tag{3.14}$$

where w_i are weights obtained from regression using seven time points across the ATP stimulated condition; w_i does not change with time. Of the pathways modeled, there is a varying degree of inflammation that results from the generation of each m_i as described by the objective function. In this particular system, the ROI for each pathway is assumed to be the amount of C_j that each

unregulated pathway can yield at each instant in time which is described by ρ_i (adapted from Straight 1994) for divergent branch points in a metabolic network.

$$\rho_i = w_i r^{kin}_{m_i \to P_i} / P_i \qquad 3.15$$

3.2.4 Estimation of the kinetic rate parameters and uncertainty analysis

The model was parameterized using data from three of the four available experimental conditions, the control, the KLA primed, and the ATP treatment cases. Data was available for the Prostaglandin and Leukotriene metabolites as an 8 point time series for the control case (7 points for the treatment cases) over a 20 hour time window. We do not have measurements for the level of PGH_2 and LTA_4 because they are unstable intermediates. Therefore, in the parameter estimation process, we optimized the profile for PGH_2 formation with the constraint that its maximum concentration remains ~10 pmol/μg DNA based on the total amount of PGs produced and a constraint was not required for LTA_4. The magnitudes of different metabolites varied from 0.001 to 10 pmol/μg of DNA. To fit the model to the data, a least squared fit error was computed from the scaled profiles of the lipid with respect to its maximum value to ensure that the varying magnitude of each metabolite's level did not skew the parameters towards the sole fit of the one metabolite with highest magnitude. The overall objective function for fitting the data was to minimize the fit-error between the experimental and the predicted metabolite concentrations [49]:

$$\min_{K,X_o} \left(\sum_{i=1}^{nsp} \left(\sum_{j=1}^{ni} \left(y_{i,j,exp} - y_{i,j,pred}(K, X_0) \right)^2 / \max\left(y_{i,j,exp}\right) \right) \right) \qquad 3.16$$

where K are the parameters or rate constants, X_0 are the initial conditions of enzyme concentrations, ni is the number of time-points, 7 (indexed as j), and nsp is the total number of species (indexed as i). The ODEs in the model were solved using ode15s for stiff systems in MATLAB (2019, Natick, MA). Parameters (Table 1) were optimized using a three-step hybrid optimization procedure that started with a heuristic search algorithm (Matlab® function "MultiStart") seeded with an initial parameter set and run up to 90 iterations to determine near optimal parameter values. The result from the application of the heuristic optimization was then further refined using a two-step local optimization approach employing a string-searching algorithm (Matlab® function "patternsearch") followed by a generalized constrained non-linear optimization employing a gradient search method (Matlab® function "fmincon").

The goodness of the fits was assessed by comparing the variance for the fitted data to the variance in the experimental (replicate) data (treatments and control data combined) using the F-test as follows [50]:

$$F = \frac{SSE_{fit} \Big/ (ne \times nt)}{SSE_{exp} \Big/ (ne \times nt \times (nr-1))} \tag{3.17}$$

$$F = \frac{\left(\sum_{j=1}^{nt}\left(Y_j^{trt} - \bar{X}_j^{trt}\right)^2 + \sum_{j=1}^{nt}\left(Y_j^{ctrl} - \bar{X}_j^{ctrl}\right)^2\right) \Big/ (ne \times nt)}{\left(\sum_{j=1}^{nt}\sum_{i=1}^{nr}\left(X_{ij}^{trt} - \bar{X}_j^{trt}\right)^2 + \sum_{j=1}^{nt}\sum_{i=1}^{nr}\left(X_{ij}^{ctrl} - \bar{X}_j^{ctrl}\right)^2\right) \Big/ (ne \times nt \times (nr-1))} \tag{3.18}$$

where Xj, $\overline{X}$j, and Yj denote the experimental data, mean experimental data, and simulated (fitted) data at time point j, respectively, nr is the number of replicates (nr = 3, indexed as i), nt is the

number of time points (nt = 7, indexed as j), ne is the number of experimental conditions used, and trt and ctrl are treatment and control groups, respectively. The degrees of freedom for determining the F distribution are $df_1 = (ne \times nt)$ and $df_2 = (ne \times nt \times (nr - 1))$. F statistic values for the fitted data smaller than $F_{0.95}(21, 42) = 1.81$ indicate statistically equal variance in simulated (fitted) and experimental data; whereas, F values smaller than $F_{0.05}(21, 42) = 0.51$ indicate the fit-error is statistically smaller than the experimental error. For the prediction case of KLA primed, ATP stimulated BMDM, F statistic values smaller than $F_{0.95}(7, 14) = 2.76$ indicate statistically equal variance in simulated and experimental data; whereas, F values smaller than $F_{0.05}(7, 14) = 0.28$ indicate the fit-error is statistically smaller than the experimental error.

3.3 Results

3.3.1.1 Relating inflammation to the cybernetic objective

As noted in previous chapters, cybernetic modeling is a goal driven approach to modeling dynamic systems. The essence of cybernetics lies in the provided goal chosen to describe the overall system behavior. Cybernetic models have their origin in the hypothesis that metabolic regulation has evolved so that cells make optimal decisions when presented with metabolic choices [89]. They integrate intracellular kinetics with an abstracted description of metabolic regulation and control. These control mechanisms are manifested as control variables that modify each kinetic rate in the model. As described previously, cybernetic models have two types of control variables, the u_i and v_i variables. The u variables are the outputs of an optimal control program managing gene expression while the cybernetic v variables control enzymatic activity. An additional cybernetic control variable has been formulated, w_i , which describes allocation of translational resources [65].

We define a local cybernetic objective to the description of different branches within the eicosanoid network which correlate with known physiological changes in immune response such as increased cytokine or chemokine levels. The prostanoids are either correlated to TNF-α (denoted as single objective) or designated as equivalently valuable (denoted as equal objective) in the onset of inflammatory signaling such that each metabolite contributes equally, and we simply define the objective as maximizing the product of all prostanoids. The leukotriene branch objective is defined based on correlation with the chemoattractant CCL2 (two objective case), which is then compared to the prostaglandin objective of TNF-α (single objective case) as the representative inflammatory cytokine, as well as a third objective in which equivalent weightage (equal weight case) is assigned to each LK in the branch. The weights of each objective designation were calculated via an ODE relation describing cytokine rate to a corresponding set of metabolites (3.2.3). In order to avoid an overfitting problem, the metabolites associated with each objective were limited to their respective branch (

Table 3.1 and Table 3.2).

Table 3.1. Calculated weights associated with the LOX metabolic network.

weight	**CCL2 objective**	**Equal objective**
w_{LTB4}	0.10	0.33
$w_{epiLTB4}$	0.63	0.33
$w_{t\text{-}epi\text{-}LTB4}$	0.27	0.33

Table 3.2. Calculated weights associated with the COX metabolic network.

weight	TNF-α objective	Equal objective
w_{PGE2}	0.15	0.25
$w_{PGF2\alpha}$	0.29	0.25
w_{PGD2}	0.33	0.25
w_{TXB2}	0.23	0.25

3.3.1.2 Simulation

To obtain the kinetic parameters, the AA metabolic network was simplified and divided into COX and LOX subnetworks similar to the division for the objective designation (Figure 3.2 detailed illustration of the intracellular signaling with eicosanoid metabolic network is shown in Figure 3.1). As an example of simplification, thromboxane A2 (TXA2) synthase (Thromboxane A synthase (TXAS)/thromboxane A synthase 1 (Tbxas1)) produces a bioactive lipid mediator, TXA2, but TXA2 is rapidly and nonenzymatically degraded to TXB2, which is measurable under our experimental condition. Therefore, the simplified network included TXB2 but not TXA2. Next, the models for both pathways were described by 24 ODEs in total and 56 parameters. The rate constants were estimated using a three-step hybrid optimization approach (3.2.4). Then, the eicosanoid profiles for the control, KLA primed, and ATP non-primed were simulated (Figure 3.3, Figure 3.4, and Figure 3.5) using three different cybernetic model objectives defined previously as TNF-α, CCL2, or equal weightage, respectively.

3.3.1.3 Prediction

To test the validity of the calculated parameters for all three of the models, we used the parameter values to predict a third independent data set, the eicosanoid profile in KLA-primed and ATP stimulated BMDM cells. When the profiles were predicted with the optimized parameter

values, the model prediction did not fit the experimental data very well. Up to 10% variability was allowed in the optimized parameter values. The range was determined from the 30% variability chosen based on previous work by our group in determining the uncertainty of the calculated parameters in the ATP-stimulated model [50]. The prediction with the relaxed bounds on the parameters for all three models yields a good fit to experimental data (Figure 3.3, Figure 3.4, and Figure 3.5). This prediction of an independent experimental dataset (KLA primed and ATP stimulated case), which was not used to fit the ATP-stimulation data, further validated the models and parameter values. The mathematical model reflects the AA metabolic network dynamics in BMDM cells.

Table 3.3 Calculated kinetic parameters for the COX pathway. The columns represent parameters calculated for each cybernetic model with either a single objective, two objectives, or no defined objective. The parameters are described as calculated parameter ± standard-error of mean (SEM) calculated from the uncertainty analysis.

**Note the (--) indicates those parameters were held the same as in the single model case.

Parameter	Single objective	Two objectives	Equal objective
kPGH2	0.0056	--	0.0050
kPGD2	0.5833	--	0.4921
kPGE2	0.0182	--	0.0062
kPGF2a	0.0025	--	0.0018
kTXB2	0.0172	--	0.0103
kdPGD2	0.0515	--	0.0520
kPGJ2	0.0205	--	0.0207
kdPGJ2	0.0362	--	0.0388
gPGH2	0.6727	--	0.4186
gPGD2	0.0095	--	0.0045
gPGE2	7.19E-07	--	1.32E-06
gPGF2a	7.21E-07	--	7.11E-07
gTXB2	7.14E-07	--	7.12E-07
gdPGD2	7.05E-07	--	7.07E-07
gPGJ2	7.18E-07	--	7.10E-07
gdPGJ2	0.0906	--	0.1032
PGH2_0	0.0080	--	0.0074
PGH2_K_0	0.9969	--	0.9999

Table 3.4 continued

Parameter	Single objective	Two objectives	Equal objective
kATP_P	4.9998	--	4.9991
KmAA	32.6344	--	48.0240
KmPG	2.3630	--	1.4908
kePGH2	0.5998	--	0.9997
kePGD2	0.9999	--	1.0000
kePGE2	0.9579	--	0.8778
kePGF2	0.4755	--	0.3786
keTXB2	0.5866	--	0.4835
ePGH2_K_0	0.9970	--	0.8286
ePGD2_K_0	0.0807	--	0.1651
ePGE2_K_0	0.0316	--	0.1622
ePGF2a_K_0	0.2659	--	0.7993
eTXB2_K_0	0.4488	--	0.5614
kLTB4	3.7248	4.9979	4.9256
kepiL	4.7975	1.7410	4.4478
ktransL	4.6567	3.6802	4.4778
kLTA4	0.0002	0.0002	0.0002
kHETE5	0.0004	0.0005	0.0005
kHETE15	0.0002	0.0001	0.0001
gLTB4	0.7044	0.9457	0.8706
gepiL	0.3519	0.2946	0.4394

Table 3.5 continued

Parameter	Single objective	Two objectives	Equal objective
gtransL	0.8269	0.8416	0.7316
gLTA4	0.3474	0.5946	0.3299
gHETE5	0.8784	0.9982	0.9668
gHETE15	0.2768	0.2438	0.2578
LTA4_0	0.0009	0.0010	0.0010
LTA4_K_0	0.0005	0.0005	0.0005
eLTB4_K_0	0.5551	0.6384	0.5566
eepiL_K_0	0.7226	0.7766	0.7405
etransL_K_0	0.7526	0.7758	0.7306
eLTA4_K_0	0.7883	0.7999	0.7975
eHETE15_K_0	0.6956	0.5995	0.6656
keLTB4	0.4857	0.1603	0.4317
keEPIL	0.2246	0.1495	0.2715
ketransL	0.3168	0.2327	0.3207
keLTA4	0.6220	0.5610	0.5733
keHETE15	0.7040	0.6085	0.6863
kATP_L	0.0017	0.0003	0.0017
kmLK	0.0139	0.0851	0.0135
beta	0.5375	0.5375	0.8909

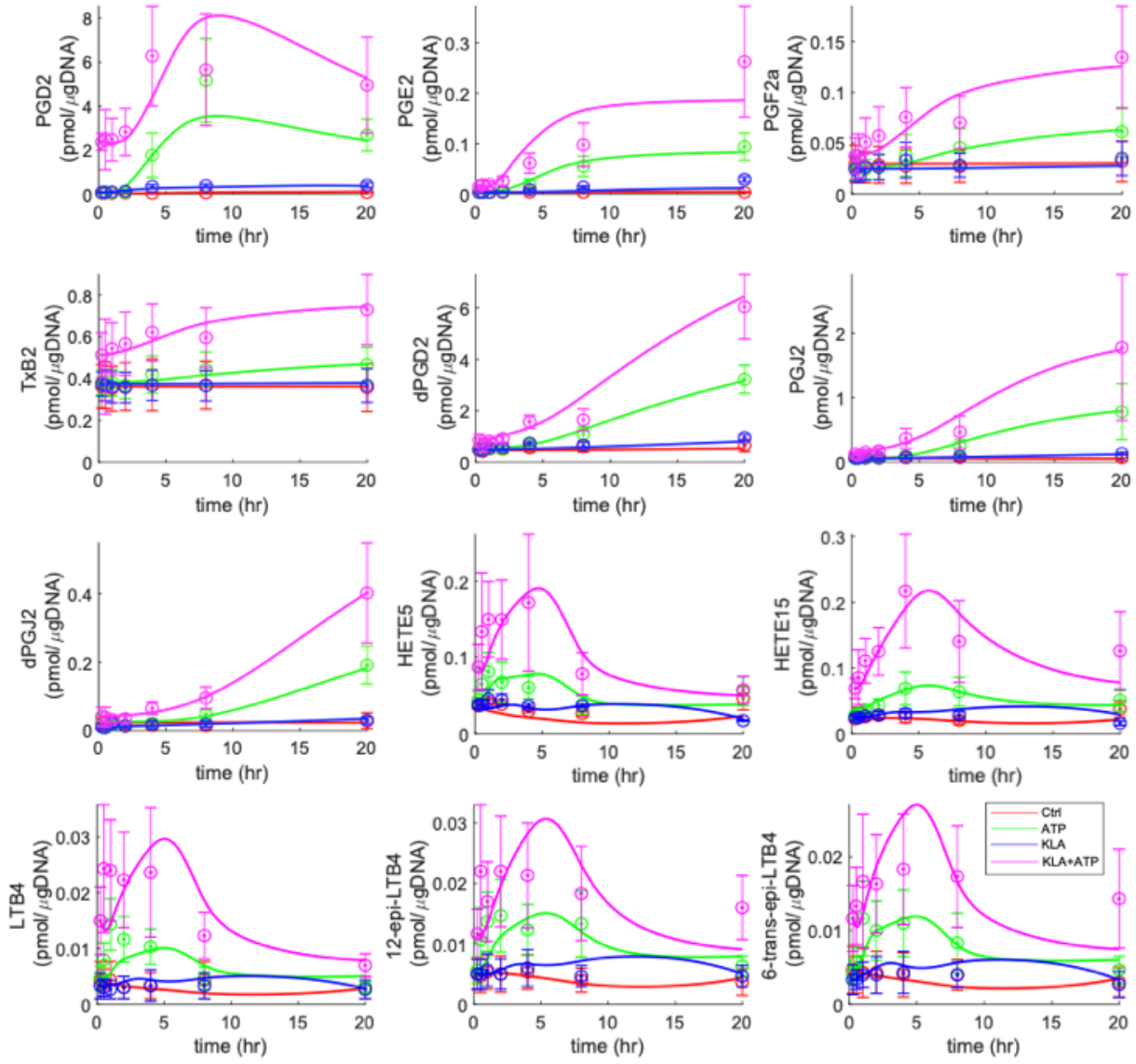

Figure 3.3. Cybernetic Simulation of Eicosanoid Levels for the Two Objective Case. The computational simulation of the eicosanoid profile is generated using the cybernetic model with the defined objective of CCL2 for the Leukotriene branch and TNF-α for the Prostaglandin branch in three different treatment conditions (control, KLA primed, and ATP stimulated BMDM) and used to predict a fourth independent data set (KLA primed/ATP stimulated). The mean experimental data (circles) with associated standard error of the mean (SEM) from three replicate experiments (n = 3) for the KLA primed (blue), ATP stimulated (green), control (red), and KLA primed/ATP stimulated (magenta) cases are taken from the mass spectrometry measurements of lipids. The simulation results are shown for the treatment and control cases (solid blue, green, and red curves, respectively) along with the prediction curve (magenta) for the combined KLA primed/ATP stimulated condition.

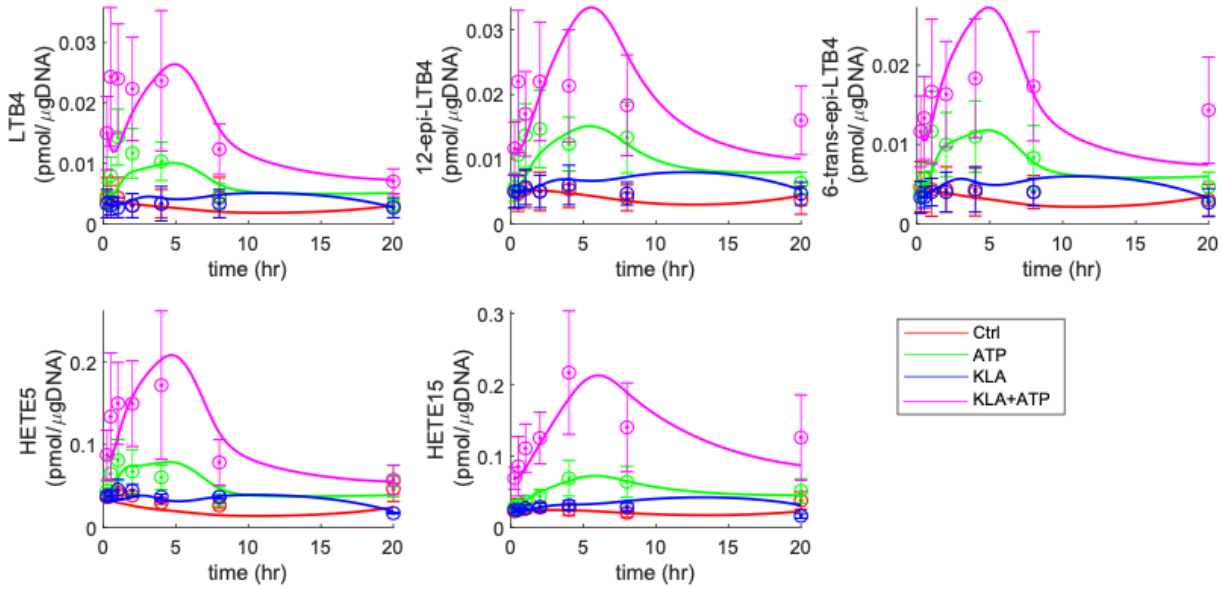

Figure 3.4. Cybernetic simulation of Leukotrienes with TNF-α as the defined cybernetic objective. The computational simulation of the eicosanoid profile is generated using the cybernetic model with the defined objective of TNF-α for the Leukotriene branch in three different treatment conditions (control, KLA primed, and ATP stimulated BMDM) and used to predict a fourth independent data set (KLA primed/ATP stimulated). The mean experimental data (circles) with associated standard error of the mean (SEM) from three replicate experiments (n = 3) for the KLA primed (blue), ATP stimulated (green), control (red), and KLA primed/ATP stimulated (magenta) cases are taken from the mass spectrometry measurements of lipids. The simulation results are shown for the treatment and control cases (solid blue, green, and red curves, respectively) along with the prediction curve (magenta) for the combined KLA primed/ATP stimulated condition.

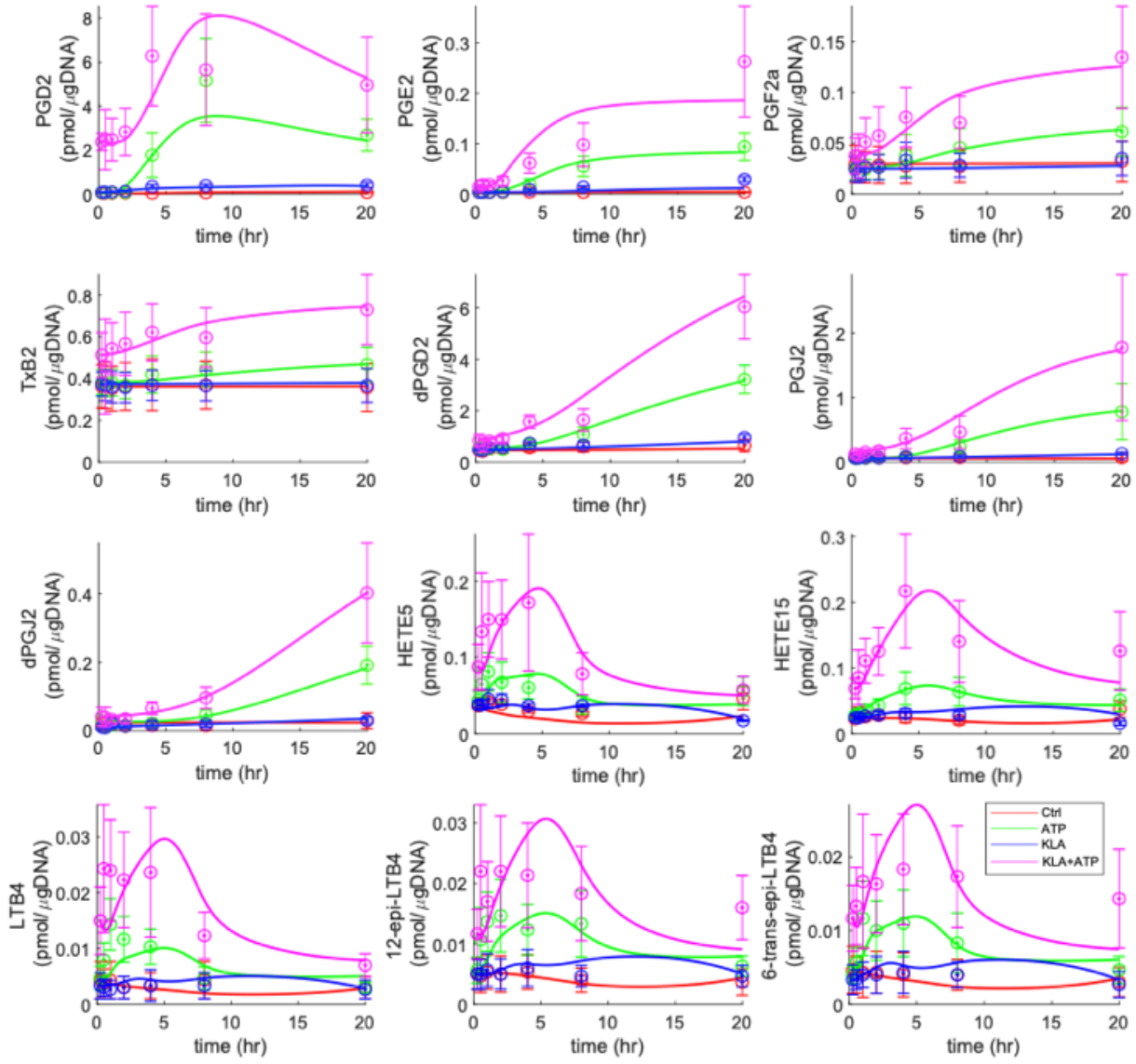

Figure 3.5. Cybernetic Simulation of Eicosanoid Levels for the Equal Weightage Cybernetic Model. The computational simulation of the eicosanoid profile is generated using the cybernetic model with the defined objective of equal weightage metabolites for the Leukotriene and Prostaglandin branches in three different treatment conditions (control, KLA primed, and ATP stimulated BMDM) and used to predict a fourth independent data set (KLA primed/ATP stimulated). The mean experimental data (circles) with associated standard error of the mean (SEM) from three replicate experiments (n = 3) for the KLA primed (blue), ATP stimulated (green), control (red), and KLA primed/ATP stimulated (magenta) cases are taken from the mass spectrometry measurements of lipids. The simulation results are shown for the treatment and control cases (solid blue, green, and red curves, respectively) along with the prediction curve (magenta) for the combined KLA primed/ATP stimulated condition.

Table 3.6. Model Accuracy for the single objective (TNF-α) model. Goodness of fit, *F*-test, for simulated/optimized (control, adenosine triphosphate (ATP) stimulated, and Kdo2-Lipid A (KLA) primed data) and predicted (Kdo2-Lipid A (KLA) primed and ATP stimulated) cases. *F* values smaller than $F_{0.05}(21, 42) = 0.51$ indicate that the fit-error is statistically smaller than the experimental error; whereas, the *F* values smaller than $F_{0.95}(21, 42) = 1.81$ indicate statistically equal variance in simulated (fitted) and experimental data.

Metabolite	**Model Fit to Data**	**Model Prediction to KLA+ATP Data**
PGD_2	0.4462	0.3171
PGE_2	0.6382	0.3082
$PGF_{2\alpha}$	0.2873	0.2551
TXB_2	0.4209	0.2803
$dPGD_2$	0.4869	0.6840
PGJ_2	0.4453	0.2142
$dPGJ_2$	0.4534	0.3430
LTB_4	0.2289	0.2792
12-epi-LTB_4	0.2462	0.2161
6-trans-epi-LTB_4	0.2350	0.2854
5-HETE	0.2865	0.2597
15-HETE	0.2842	0.3189

Table 3.7. Model accuracy for Leukotriene branch with CCL2 objective. Goodness of fit, *F*-test, for simulated/optimized (control, adenosine triphosphate (ATP) stimulated, and Kdo2-Lipid A (KLA) primed data) and predicted (Kdo2-Lipid A (KLA) primed and ATP stimulated) cases. *F* values smaller than $F_{0.05}(21, 42) = 0.51$ indicate that the fit-error is statistically smaller than the experimental error; whereas the *F* values smaller than $F_{0.95}(21, 42) = 1.81$ indicate statistically equal variance in simulated (fitted) and experimental data.

Metabolite	**Model Fit to Data**	**Model Prediction to KLA+ATP Data**
LTB_4	0.2394	0.1992
12-epi-LTB_4	0.2422	0.2896
6-trans-epi-LTB_4	0.2306	0.2958
5-HETE	0.2902	0.3350
15-HETE	0.2861	0.3011

Table 3.8. Model accuracy for equal weightage cybernetic model of eicosanoid metabolism. Goodness of fit, *F*-test, for simulated/optimized (control, adenosine triphosphate (ATP) stimulated, and Kdo2-Lipid A (KLA) primed data) and predicted (Kdo2-Lipid A (KLA) primed and ATP stimulated) cases. *F* values smaller than $F_{0.05}(21, 42) = 0.51$ indicate that the fit-error is statistically smaller than the experimental error; whereas the *F* values smaller than $F_{0.95}(21, 42) = 1.81$ indicate statistically equal variance in simulated (fitted) and experimental data.

Metabolite	**Model Fit to Data**	**Model Prediction to KLA+ATP Data**
PGD_2	0.4382	0.3320
PGE_2	0.6202	0.3861
$PGF_{2\alpha}$	0.2850	0.2568
TXB_2	0.4204	0.2847
$dPGD_2$	0.4813	0.8027
PGJ_2	0.4347	0.2263
$dPGJ_2$	0.4421	0.3568
LTB_4	0.2330	0.2792
12-epi-LTB_4	0.2473	0.2161
6-trans-epi-LTB_4	0.2321	0.2854
5-HETE	0.2890	0.2597
15-HETE	0.2833	0.3189

The eicosanoid model robustness was evaluated by performing a parametric sensitivity analysis in which each parameter was varied individually by +/- two-fold of the original optimized value. The slope of each parameter and metabolite sensitivity curve was calculated to evaluate the sensitivity. A heat map of the slopes was then generated. Small to moderate sensitivities in most of the parameters were observed. As expected, very little or no variation in the degradation parameters is seen in response to metabolite changes. Based on these results, our models of eicosanoid metabolism are shown to be robust with respect to parametric perturbations.

3.4 Discussion

3.4.1 Understanding the role of regulation in the cybernetic variables

Eicosanoids are derived from arachidonic acid (AA), a 20-carbon fatty acid, and are further classified into prostaglandins, thromboxanes, leukotrienes, and other oxidized products [47]. PGs have been found to mediate pain, fever, and other symptoms associated with inflammation [48]. Prostanoids thus formed are immediately released outside of the cell, with little if any of the product remaining in the cell. Because they are either chemically or metabolically unstable, prostanoids work only locally, near their site of production. PGI_2 and TXA_2 spontaneously degrade into inactive compounds under physiological conditions, and other PGs are enzymatically inactivated during a single passage through the lung. In addition, PGD_2 and PGE_2 are slowly dehydrated in biological fluids containing serum albumin to yield the cyclopentenone PGs, PGA_2 and PGJ_2, which contain an unsaturated ketone. Evaluating the role of regulation as it appears in our model results allows us to relate the significance of our model to biologically relevant mechanisms.

3.4.1.1 u and v dynamics (biological significance)

Two prominent features of acute inflammation are vasodilation and pain generation which are attributed to prostanoid contributions. The profiles of prostanoids generated in an inflammatory site change during the course of inflammation and are also dependent on the stimulus and site of inflammation [6]. In pain, the PGs are involved in both hyperalgesia, an increased sensitivity to a painful stimulus, and allodynia, a pain response to a usually nonpainful stimulus.

Additionally, systemic illnesses are typically associated with fever, loss of appetite, fatigue, and the induction of slow-wave sleep, among others. PGD2 is synthesized in both the central nervous system (CNS) and peripheral tissues; it both inflammatory and homeostatic functions.

[101]. PGD_2 in the brain tissue is involved in the regulation of sleep and other CNS activities, which also includes pain perception [102, 103]. Given the role of PGD_2 in sleep cycles, it likely contributes to the drowsiness associated with systemic illness [102].

The lipid of specific interest to the inflammatory response is PGE_2 because it plays a role in all processes that lead to the classic signs of inflammation. PGE_2 is the most abundant PG detected in various tissues and is known to have bone-resorptive activity and to mediate bone resorption induced by cytokines and LPS. Pathological and physiological actions of PGE_2 occur via four sub- types of PGE receptors, termed E-type prostanoid receptor 1–4 (EP1–4) which are expressed in the cell surface membrane and each receptor is associated with a distinct signal transduction pathway. PGE_2 is involved in the induction of acute inflammation and induces redness, heat, and swelling reactions by relaxing vascular smooth muscle and increasing blood flow via the EP2/EP4 receptors. Pain is a result of the action of PGE_2 on sensory neurons found in the periphery as well as on central sites within the brain and spinal cord [37]. Additionally, hyperalgesia, an enhanced sensitivity to pain and classic sign of inflammation, is mediated mainly by PGE_2 through the EP1 receptor signaling that acts on these sensory neurons at the site of inflammation [55]. We see that PGE_2 regulates various steps of inflammation in a context-dependent manner and takes on both pro-inflammatory and anti-inflammatory properties proving a critical player in the inflammatory response.

$PGF_{2\alpha}$ is primarily derived from COX-1 in the female reproductive system and is a critical player in ovulation and contraction of the smooth muscle of the uterus. Findings show that $PGF_{2\alpha}$ plays a significant role in renal function, arterial contraction, myocardial dysfunction, brain injury, and pain [146-151]. Biosynthesis of $PGF_{2\alpha}$ *in vivo* is found in larger quantities in basal physiological conditions, as well as certain physiological and pathophysiological situations like

acute and chronic inflammation, in both the peripheral plasma and urine [143]. Increased synthesis of $PGF_{2\alpha}$ has been reported in patients suffering from various forms of arthritis [159]. Elevated levels of $PGF_{2\alpha}$ have also been associated with cardiovascular risk factors along with increased levels of IL-6 and acute phase proteins in body fluids [160, 161].

The prostanoid TXA_2 is an unstable AA metabolite with a half-life of about 30 seconds is non-enzymatically degraded into biologically inactive TXB_2. TXA_2 is predominantly derived from platelet COX-1, as well as in other cell types including by macrophage COX-2 [164, 165]. The principle vasoactive product of COX-1 in platelets is TXA_2. In addition, TXA_2 along with several other eicosanoids, PGE_2 and PGI_2, may contribute to regulation of systemic blood pressure.

Leukotrienes are known pro-inflammatory mediators that contribute to pathophysiologic features of asthma, such as airway smooth muscle contraction, increase in microvascular permeability, stimulation of mucus secretion, and recruitment of eosinophils into the airways [125]. In particular, LTB_4 selectively affects neutrophil functions and recruitment into the lung, where it has the capacity to activate these cells, resulting in inflammation. LTB_4 may also be involved in inflammatory pain by reducing the nociceptive threshold via neutrophil signaling [8].

From this information, we would expect that PGE_2 and PGD_2 synthesis and activity (Figure 3.6) remain highest relative to their neighboring branched metabolites also being regulated by the cybernetic control variables. At the basal state, the enzyme levels for Ptges1 are higher than that for Ptgds2 (Figure 3.6). The flux through Ptges1 provides the highest cybernetic control across all four prostanoids as the system's initial response to infection. As the enzyme Ptgds2 increases, we see a switch in the cybernetic control for an enhanced inflammatory response. The cybernetic regulation of PGF_{2a} and TXB_2 enzymes are not as prominent as PGE_2 and PGD_2 enzymes; however, we do see an increase in cybernetic regulation of those enzymes (Figure 3.6). The higher

basal level of Ptges1 compared to that of Ptgds2 is also corroborated in our micro-array expression data and in publicly available tissue RNAseq dataset. We know that PGE_2 and PGD_2 are known mediators in the inflammatory response particularly during the acute phase of inflammation. Similarly, for the Leukotriene branch, we note the enzymes associated with LTB4 and 6-trans-12-epi-LTB4 are most active in the branch. We again see a switch in the prioritization of metabolite production between these two competing products in the models (Figure 3.8 and Figure 3.8).

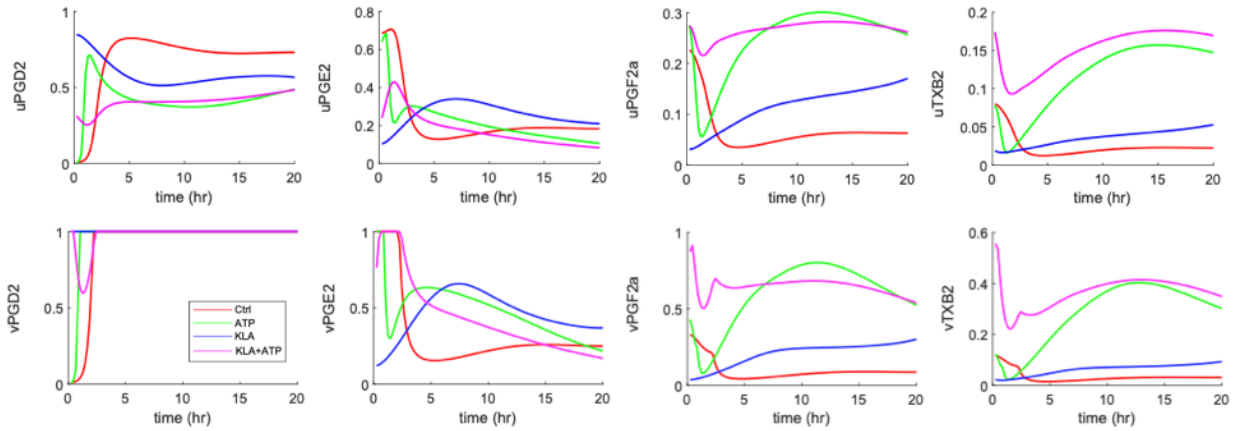

Figure 3.6. Cybernetic control variables u and v for the Prostaglandin branch in the single objective case.

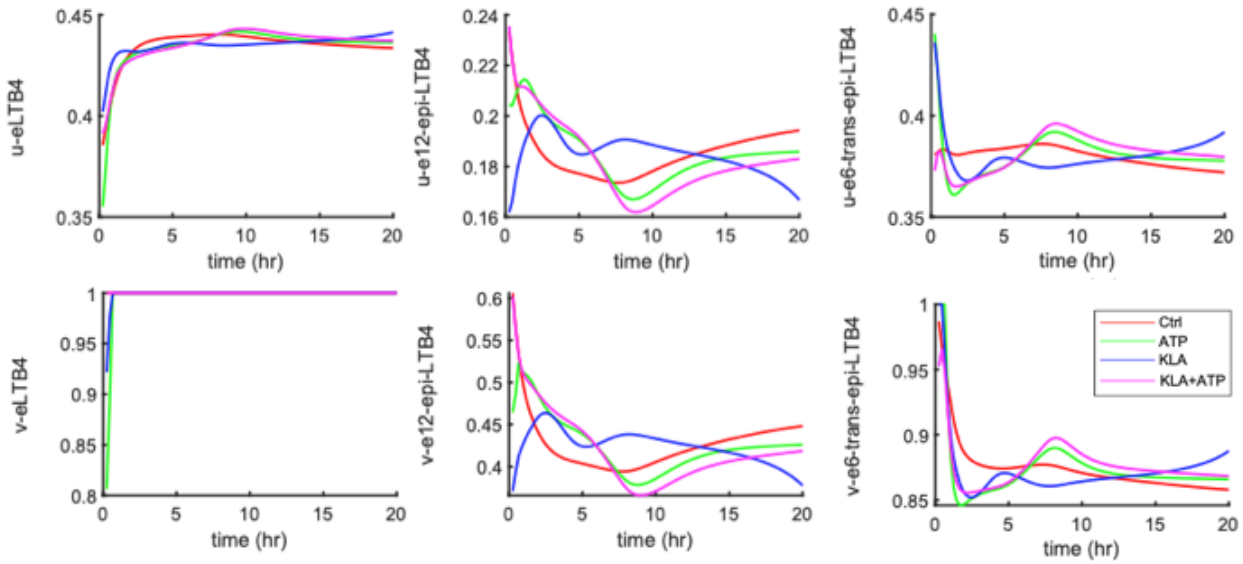

Figure 3.7. Cybernetic control variables u and v for the Leukotriene branch in the single objective case.

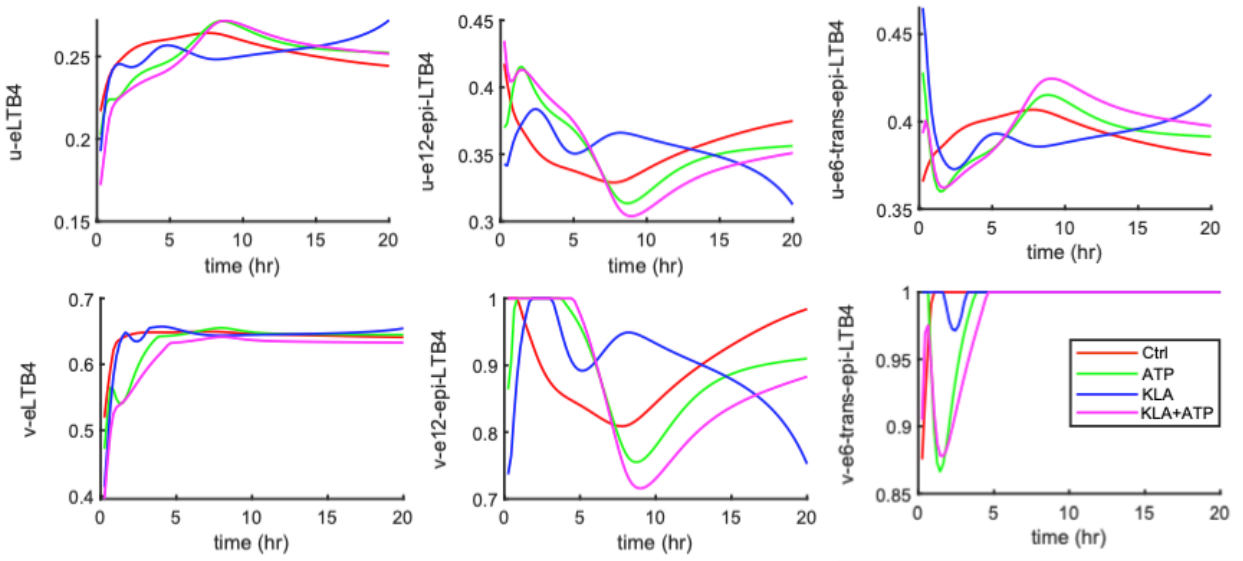

Figure 3.8. Cybernetic control variables u and v for the Leukotriene branch in the two-objective case.

3.4.1.2 Comparison of model flux to literature

To confirm the reliability of calculated rate constants, the effective rate constant for the enzymes COX (EC 1.14.99.1), PGDS (EC 5.3.99.2), and PGES (EC 5.3.99.3) were compared with the corresponding values reported in the literature [33–36]. Since the concentrations in the LIPID MAPS experimental data and literature values were reported in units of pmol/mgDNA and mmol/min/mg of enzyme-enriched protein, respectively, we used appropriate conversion factors, assuming the cell diameter to be 10mm and other relevant information about the average cell density, percentage protein content, and total percentages of RNA and mRNA per cell. For the amount of COX protein per cell, we used COX mRNA/total RNA data from Chan et al. [37] and assumed that this ratio is the same at the protein level. The values reported in the literature were based on *in vitro* measurements with partially purified protein. Thus, we assumed that the literature values represented basal activity and compared these activities (flux through the enzyme) for predicted activities of these enzymes in the control and treated simulations to provide an expected range. For example, our computed range for COX includes the reported value (10^{-14} mmol/min/cell) [37]. A comparison between the simulated and experimental values for all three enzymes is shown in Table 3.9. The finding that the flux distribution between PGD_2 and PGE_2 pathways is comparable to previous reports has an important implication for the validity of the computational model.

Table 3.9. Comparison of computed enzyme activities with the corresponding literature values.

Enzyme (EC No.)	Literature Value (μmol/ min/mg protein)	Literature Value (μmol/ min/cell)	Single objective (μmol/ min/cell)	Two objective (μmol/ min/cell)	Equal objective (μmol/ min/cell)
COX (EC 1.14.99.1)	3.96	10^{-14}	10^{-14}- 10^{-13}	--	10^{-14}- 10^{-13}
Ptges (EC 5.3.99.3)	2	10^{-15}	10^{-18} - 10^{-15}	--	10^{-17}- 10^{-15}
Hpgds/Ptgds2 (EC 5.3.99.2)	1.7	10^{-14}	10^{-17} - 10^{-14}	--	10^{-16}- 10^{-14}

3.4.2 Model perturbation analysis

Three different perturbations were performed on different branches of the eicosanoid network to assess variations between the cybernetic models. A perturbation of ATP translates to a perturbation to the COX enzyme which can come in the form of a non-steroidal anti-inflammatory drug (NSAID), such as Aspirin. Other perturbations to the system come downstream of this and result in perturbations to enzymes at the branches in the network where we employ the cybernetic control variables. Two separate perturbations were performed on two different enzymes targeting the COX pathway with Ptgds2 (the enzyme associated with PGD_2 production) and the LOX pathway with LTA4h (the enzyme associated with LTB_4 production) inhibition through simulated chemical knockdown (mock drug response) and gene-knockdown studies.

3.4.2.1 ATP reduction

A system perturbation to the ATP results in down regulation of the COX enzyme and consequently results in down regulation of all associated metabolites in the prostanoid branch of the network. The curves associated with the single objective (green) and equal weights (black)

models show little to no variation between the models (Figure 3.9). This is likely attributed to the similarity between the objective weights (Table 3.2) defined between the two models for the PG branch. For the LK branch, we see a decrease in LK metabolites when a similar perturbation is applied impacting the initial ATP input to the system for that part of the network. From these plots (Figure 3.9) we can see the LK branch shows a variation in metabolite levels for the metabolites specifically associated with the cybernetic control variables. If we refer to the plot for LTB4, for example, we notice that the red curve representing the two objective case, or the CCL2 chemokine associated with the leukotriene branch, decreases as the suppression of the COX enzyme increases (Figure 3.10). If we look at metabolites not regulated by the cybernetic control variables (e.g., 5-HETE and 15-HETE) we notice that the differences between cybernetic models during a perturbation are not seen (Figure 3.9). This confirms our hypothesis and expectation that the weight associated with each branched metabolite impacts the resulting cybernetic formulation.

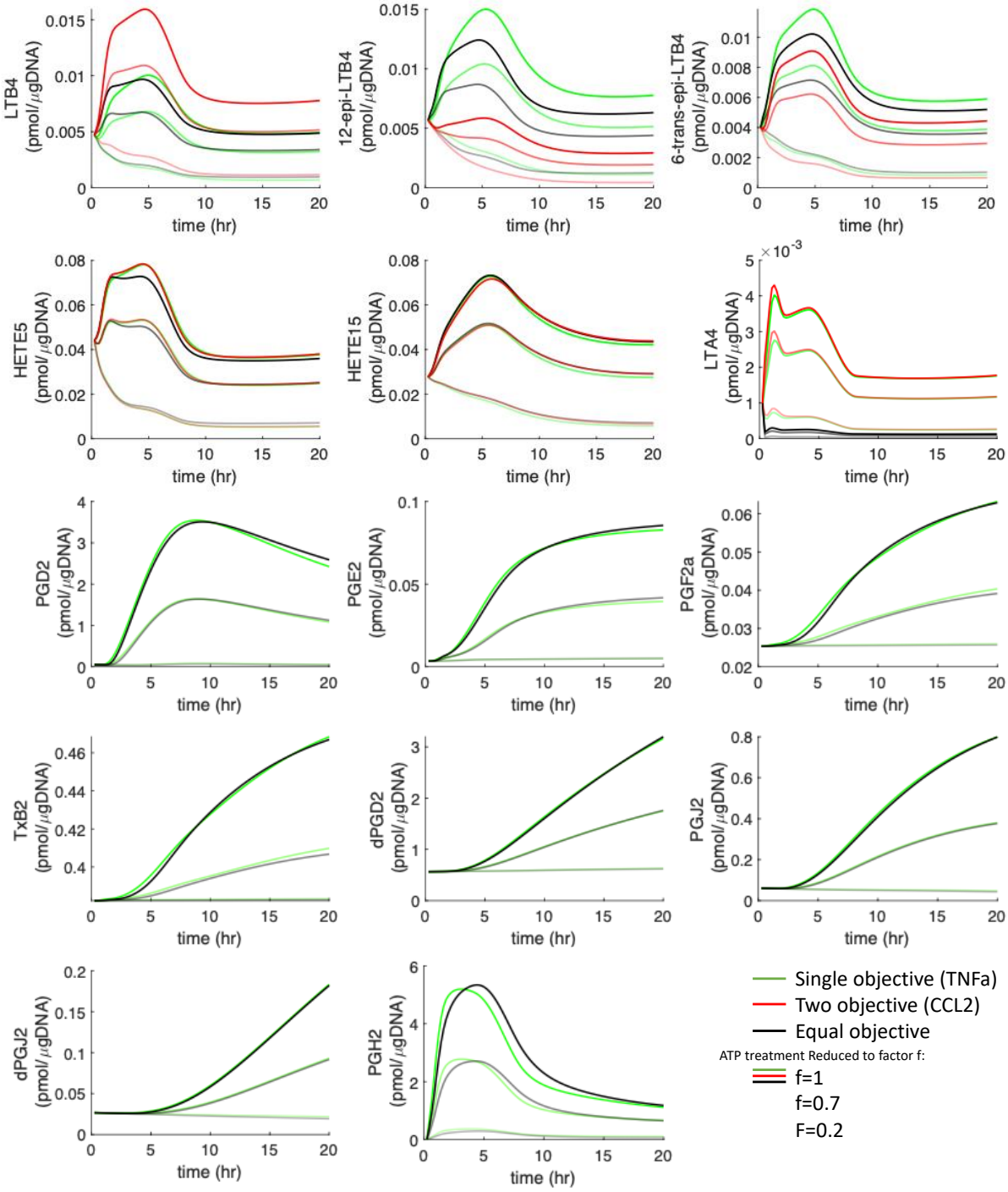

Figure 3.9. Eicosanoid metabolite levels simulated by a reduction in ATP to the system.

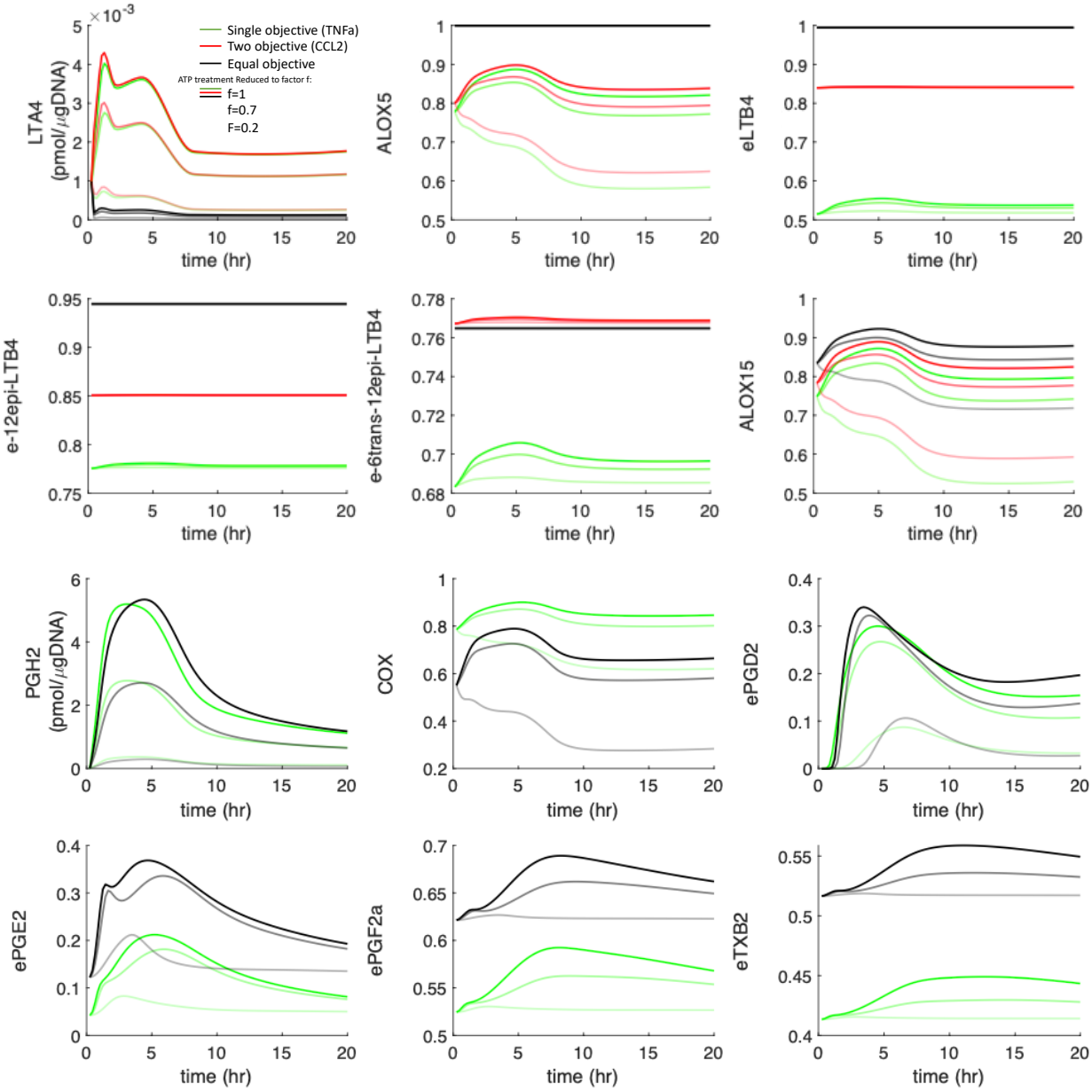

Figure 3.10. Relative enzyme levels of Eicosanoids simulated by a reduction in ATP to the system.

3.4.2.2 Enzyme activity suppression: Mimicking a drug response

A targeted drug dose to suppress a specific enzyme in the eicosanoid network corresponds to a suppression in the specific enzyme's activity. A simulated enzyme perturbation to the PGD2 branch of the network results in down regulation of the Ptgds2 enzyme and consequently results in down regulation of all associated metabolites in the prostanoid branch of the network (Figure 3.10). Similarly, we see a decrease in leukotriene metabolites when an enzyme perturbation is applied impacting a branch in that part of the network. From the perturbation plots (Figure 3.10), we can see the leukotriene branch shows a variation in metabolite levels for the metabolites specifically associated with the cybernetic control variables. If we again refer to the plot for LTB4, for example, we notice that the red curve representing the two objective case, or the CCL2 chemokine associated with the leukotriene branch, decreases as the suppression of the LTA4h enzyme increases (eLTB4 goes down, Figure 3.12). If we look at metabolites not regulated by the cybernetic control variables (e.g., 5-HETE and 15-HETE) we notice that the differences between cybernetic models during a perturbation are not seen (Figure 3.11). This confirms our hypothesis and expectation that the weight associated with each branched metabolite impacts the resulting cybernetic formulation.

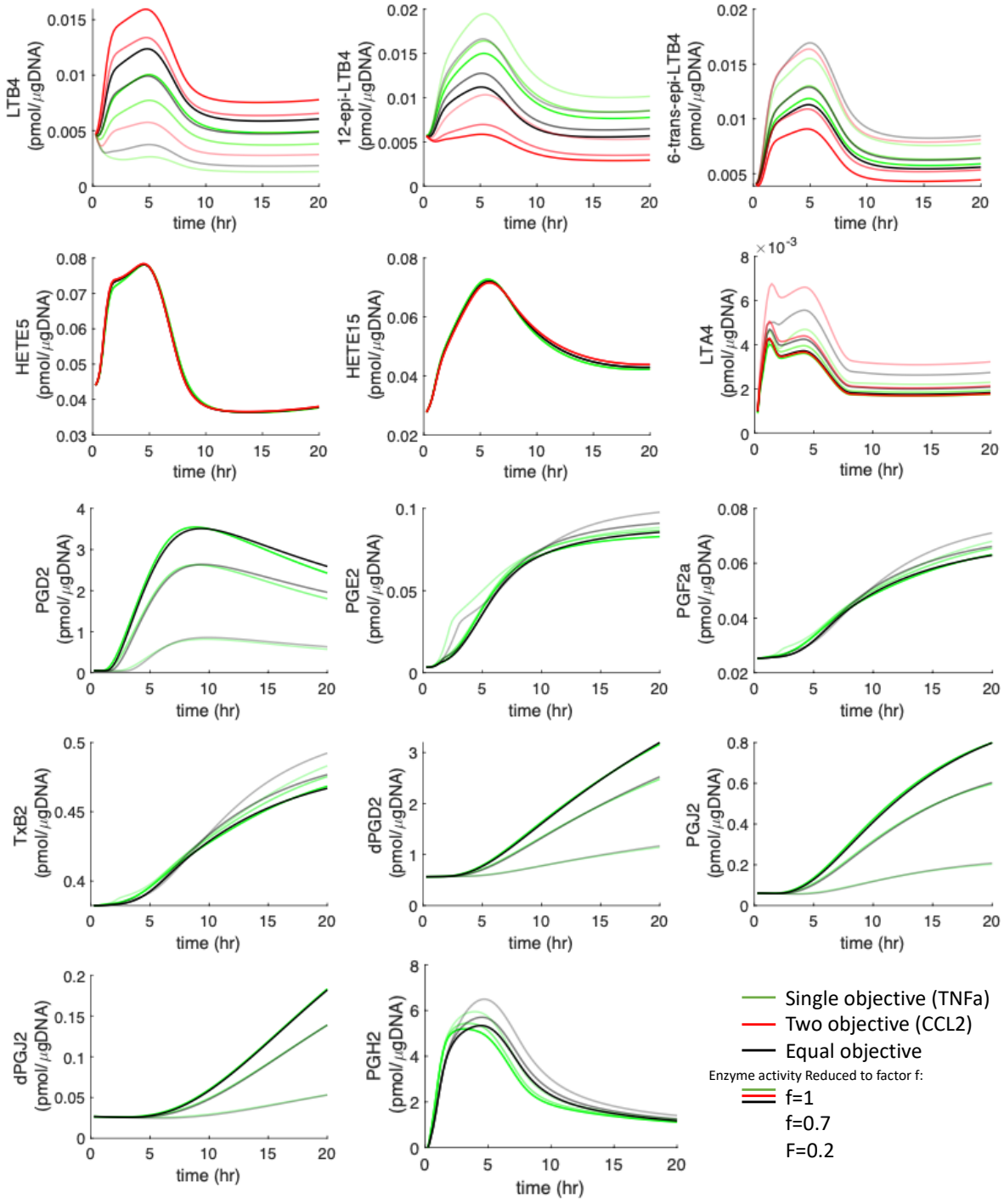

Figure 3.11. Eicosanoid metabolite levels for a simulated drug targeted response to PGE2 and LTB4 by an induced chemical suppression of enzyme activity for Ptges1 and LTA4h, respectively.

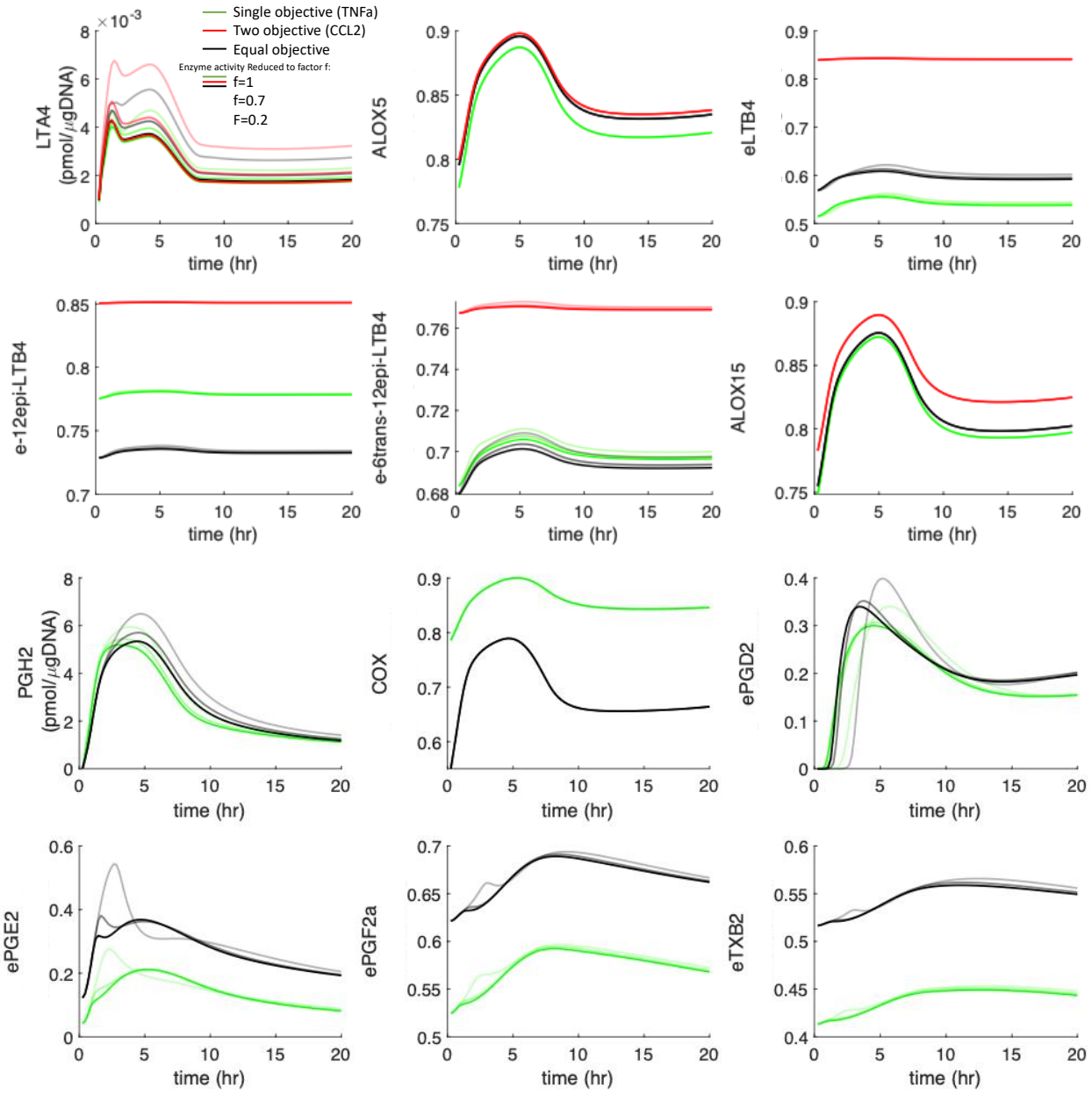

Figure 3.12. Relative enzyme levels of Eicosanoids for a simulated drug targeted response to PGE2 and LTB4 by an induced chemical suppression of enzyme activity for Ptges1 and LTA4h, respectively.

3.4.2.3 Enzyme synthesis suppression: Mimicking a gene knockdown study

A gene knockdown study to suppress a specific enzyme in the eicosanoid network corresponds to a suppression in the specific enzyme's synthesis. A simulated enzyme perturbation to the PGD2 branch of the network results in down regulation of the Ptgds2 enzyme and

consequently results in down regulation of all associated metabolites in the prostanoid branch of the network. Similarly, we see a decrease in leukotriene metabolites when an enzyme perturbation is applied impacting a branch in that part of the network. From the perturbation plots (Figure 3.13), we can see the leukotriene branch shows a variation in metabolite levels for the metabolites specifically associated with the cybernetic control variables. If we refer to the plot for LTB4, for example, we notice that the red curve representing the two objective case or the CCL2 chemokine associated with the leukotriene branch we see those levels decrease as the suppression of the LTA4h enzyme increases (Figure 3.14, graph labeled eLTB4). If we look at metabolites not regulated by the cybernetic control variables (e.g., 5-HETE and 15-HETE) we notice that the differences between cybernetic models during a perturbation are not seen (Figure 3.13). This confirms our hypothesis and expectation that the weight associated with each branched metabolite impacts the resulting cybernetic formulation.

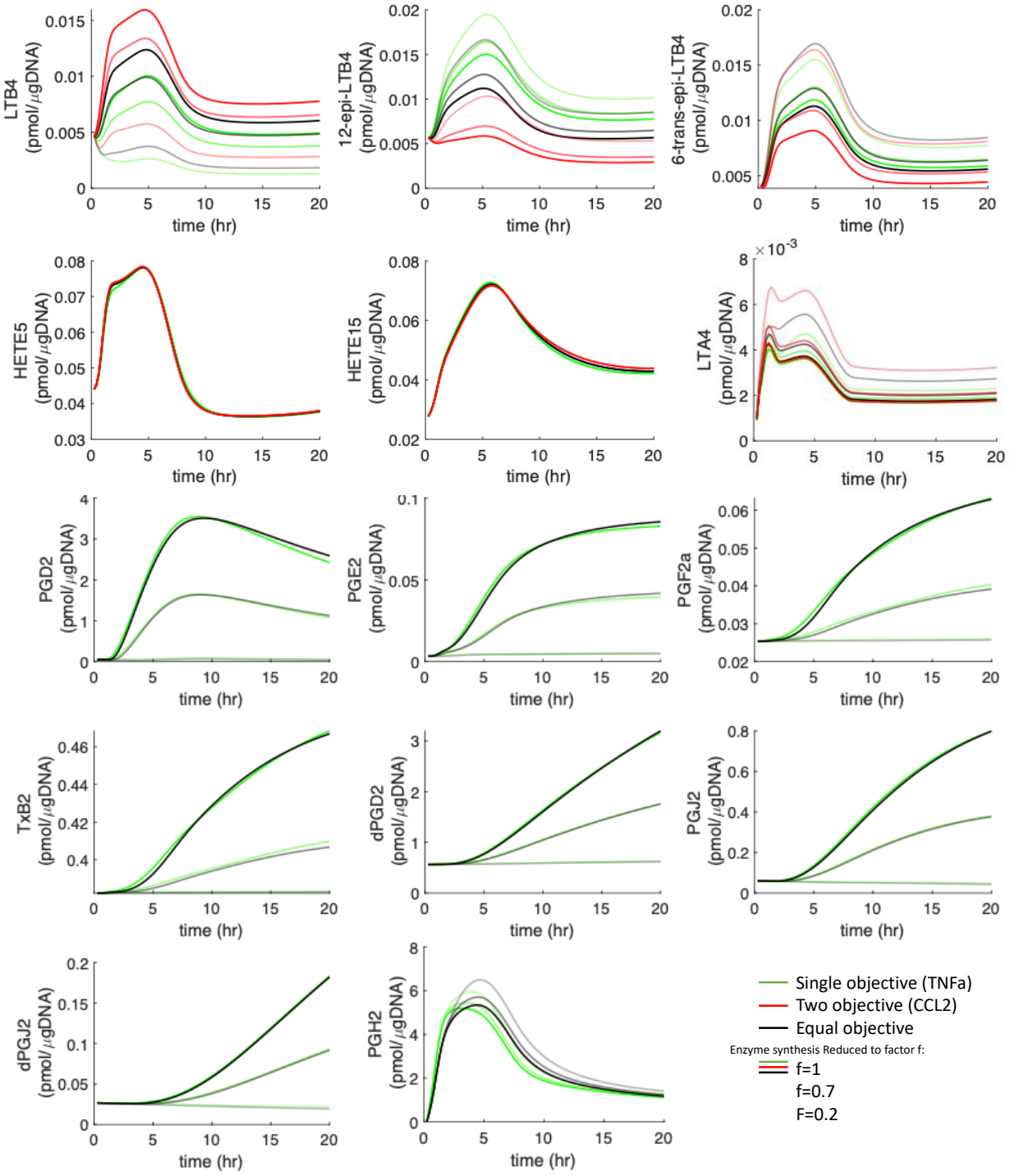

Figure 3.13. Eicosanoid metabolite levels for a simulated gene knockdown response for PGE2 and LTB4 by an induced suppression of enzyme synthesis of Ptges1 and LTA4h, respectively.

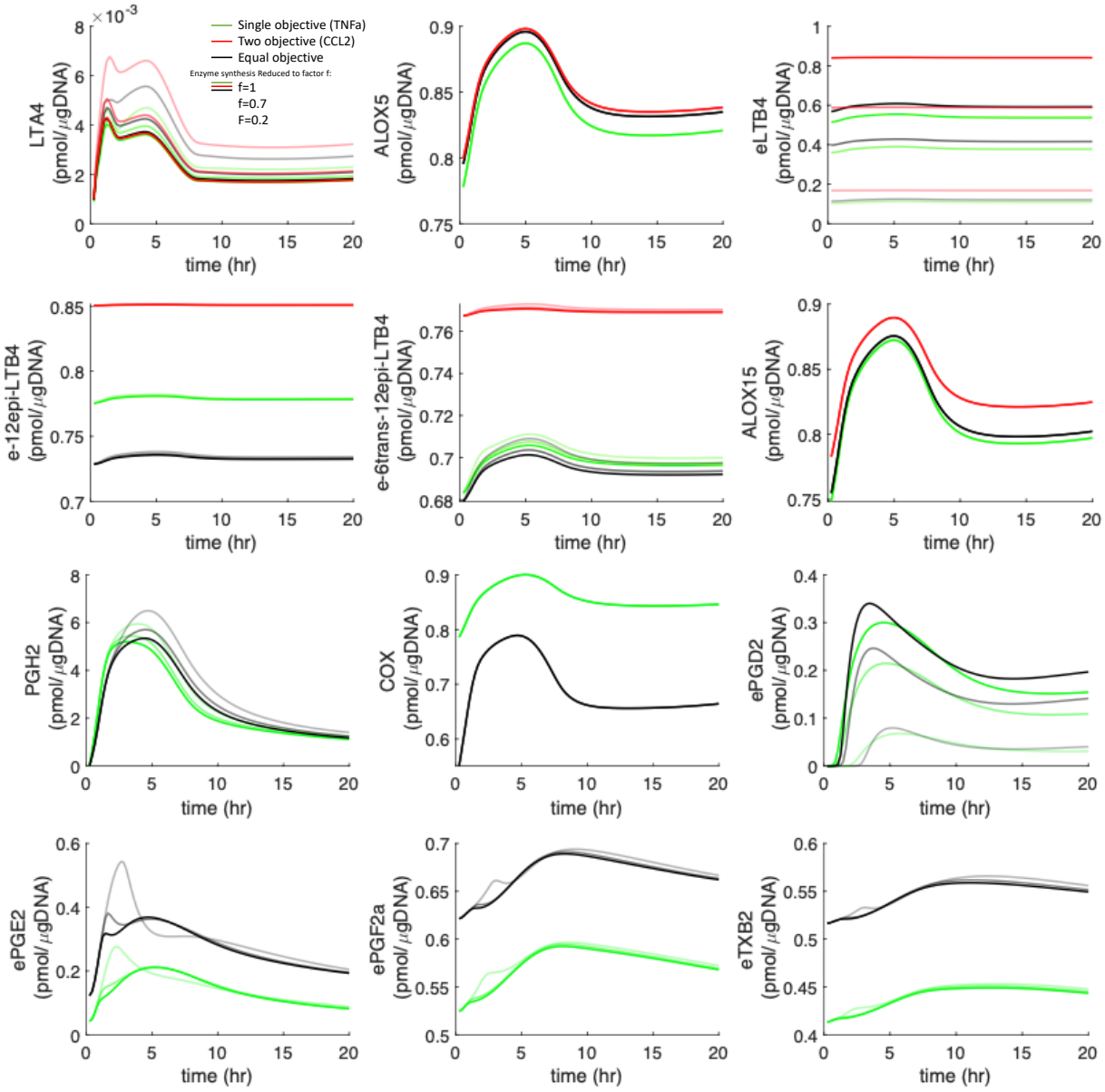

Figure 3.14. Relative enzyme levels of Eicosanoids for a simulated gene knockdown response for PGE2 and LTB4 by an induced suppression of enzyme synthesis of Ptges1 and LTA4h, respectively.

3.5 Concluding remarks

The process of inflammation is mediated by the production of multiple cytokines, chemokines, lipid mediators, etc. each of which contribute to specific individual objectives. For such complex processes in mammalian systems, a cybernetic objective based on a single

protein/component may not be sufficient to capture all the biological process thereby necessitating the use of multiple objectives. The choice of the objective function has been made by intuitive considerations in this Chapter. If objectives are conjectured, an argument can be made for numerous alternatives. Since regulatory effects are estimated from unregulated kinetics, one encounters the risk of multiplicity in this regard giving rise to multiple models. The best model is of course that which is able to predict a comprehensive set of perturbations. Here, we have extended our model in Chapter 2 to also capture the dynamics of LKs. We have used migration as a biological goal for LK using the chemoattractant CCL2 as a key representative molecule describing cell activation leading to an inflammatory response where a goal composed of multiple cybernetic objectives is warranted. Alternative model objectives included relating both branches of the eicosanoid metabolic network to the inflammatory cytokine TNF-α, as well as simply maximization of all metabolic products such that each equally contributes to the inflammatory system outcome.

We were again able to show that all three cybernetic objectives describing the LK and PG branches for eicosanoid metabolism capture the complex regulation and provide a reliable description of eicosanoid formation. We performed simulated drug and gene perturbation analyses on the system to identify differences between the models and found all cybernetic models (indicated by red, green, and black curves) show similar trends. Based on statistical analysis of the data and associated error with the models, we find that all three models provide statistically significant good fits to the data as well as are able to capture the prediction scenario of KLA+ATP reasonably well. If we look at the LK branch, we see what appears to be significant variations between the models but we are unable to differentiate whether these differences are statistically significant such that we can say they are in fact attributed to the model variations or are an artifact

of the associated measured experimental errors. Nevertheless, the cybernetic theory should not take on the burden of this uncertainty. It is still worth noting that the cybernetic framework holds and is able to capture the dynamics of the system.

In the equal objective case, we are defining the weights of the system to be equivalent, thereby stating the cybernetic objective is simply a maximization of the branching products. In relating the immune system to the actual objective, there is a hypothesis buried in that definition. The underlying hypothesis is based on the fact that we must produce all these metabolites in such a way that all the metabolites are equally important in their role in the inflammatory response. The inflammation is maximized by the joint production of all the involved prostanoids. Because all are important, we can not exclude any one of the metabolites. We see that all three models capture the metabolite levels effectively; however, the corresponding enzyme levels and regulatory control variables highlight distinct differences. Additional experiments that induce differences in the metabolic outcomes of the eicosanoids to select the best cybernetic model are necessary. In particular, capturing the LK dynamics and repeating existing experiments to reduce the error associated with that branch will be critical in allowing for differences in cybernetic models to emerge.

4 EXTENSION OF THE CYBERNETIC FRAMEWORK AND APPLICATION TO OTHER SYSTEMS

4.1 Summary

In the following sections, we explain the cybernetic modeling framework through an example and highlight the extensibility of the cybernetic framework to other complex biological systems.

4.2 The proposed cybernetic framework for applications in mammalian systems

Cybernetic modeling defines the cybernetic objective which accounts for regulatory processes in the cell based on optimizing an organism's goal. The model achieves its cybernetic objective by controlling the level of key enzymes using cybernetic control variables for induction of enzyme synthesis (u) and modulation of enzyme activity (v). A schematic to develop the cybernetic model for a metabolic network and estimate the unknown parameters (p) is presented in Figure 4.1. The trained model can then be used to predict novel scenarios. Here, we present a generic formulation of the cybernetic framework where it is applied to a specific node in the metabolic network.

4.2.1 Determining the cybernetic equations/formulation

The cybernetic framework views each branch of the pathway as a metabolic route to achieve a designated objective and describes metabolic regulation in terms of their optimal combinations. Metabolic networks can be comprised of specific decision points where a substrate metabolite M_s is converted to $\underline{n}$ product metabolites M_i in the presence of enzymes e_i.

$$M_s \xrightarrow{e_i} M_i \text{ where } i = 1 \; to \; n \tag{4.1}$$

The rate of production of M_i from M_s can be written as:

$$r_{M_s \to M_i} = r_{M_i}^{kin} \varepsilon_i v_i \tag{4.2}$$

where $r_{M_i}^{kin}$ is a function of the substrate M_s and represents the unregulated rate to produce M_i; ε_i represents relative e_i concentration with respect to a theoretical maximum e_i concentration; v_i is the cybernetic variable controlling enzyme activity. The metabolite levels are determined from the following relation (the "Model" block in Figure 4.1):

$$\frac{dM_i}{dt} = r_{M_i}^{kin} v_i \varepsilon_i - \gamma_i M_i \tag{4.3}$$

where γ_i is the degradation rate constant. The enzyme and relative enzyme level, e_i and ε_i, respectively, are governed by the following equations:

$$\frac{de_i}{dt} = \alpha + r_{e_i}^{kin} u_i - \beta e_i \tag{4.4}$$

$$\frac{d\varepsilon_i}{dt} = \beta \frac{\alpha + r_{e_i}^{kin} u_i}{\alpha + \max\left(r_{e_i}^{kin}\right)} - \beta \varepsilon_i \tag{4.5}$$

$$\text{where} \quad \varepsilon_i = \frac{e_i}{\max(e_i)} \quad and \quad \max(e_i) = \frac{\alpha + \max\left(r_{e_i}^{kin}\right)}{\beta} \tag{4.6}$$

where u_i is the cybernetic variable regulating the rate of enzyme synthesis. The three terms on the right-hand side denote the constitutive rate α, the maximum inducible rate $r_{\varepsilon_i}^{kin}$ of enzyme synthesis modulated by cybernetic variable u_i, and the decrease of enzyme level through degradation defined by the rate constant β.

4.2.2 Defining the cybernetic objective

In the standard cybernetic framework, the defined biological goal is maximization of biomass or carbon uptake rate. However, for complex mammalian systems, the system goal may be different. For example, during infection, the initial goal of the system may be to maximize the inflammatory response. The work by Aboulmouna et al. adapted the cybernetic framework described above to model AA metabolism in inflamed macrophages [33]. Macrophages are known as cytokine factories and express various cytokines in response to inflammation. Cytokines facilitate communication within the immune system. Tumor necrosis factor (TNF)-α is an exemplary pro-inflammatory cytokine and was designated as a cybernetic objective for modeling AA metabolism.

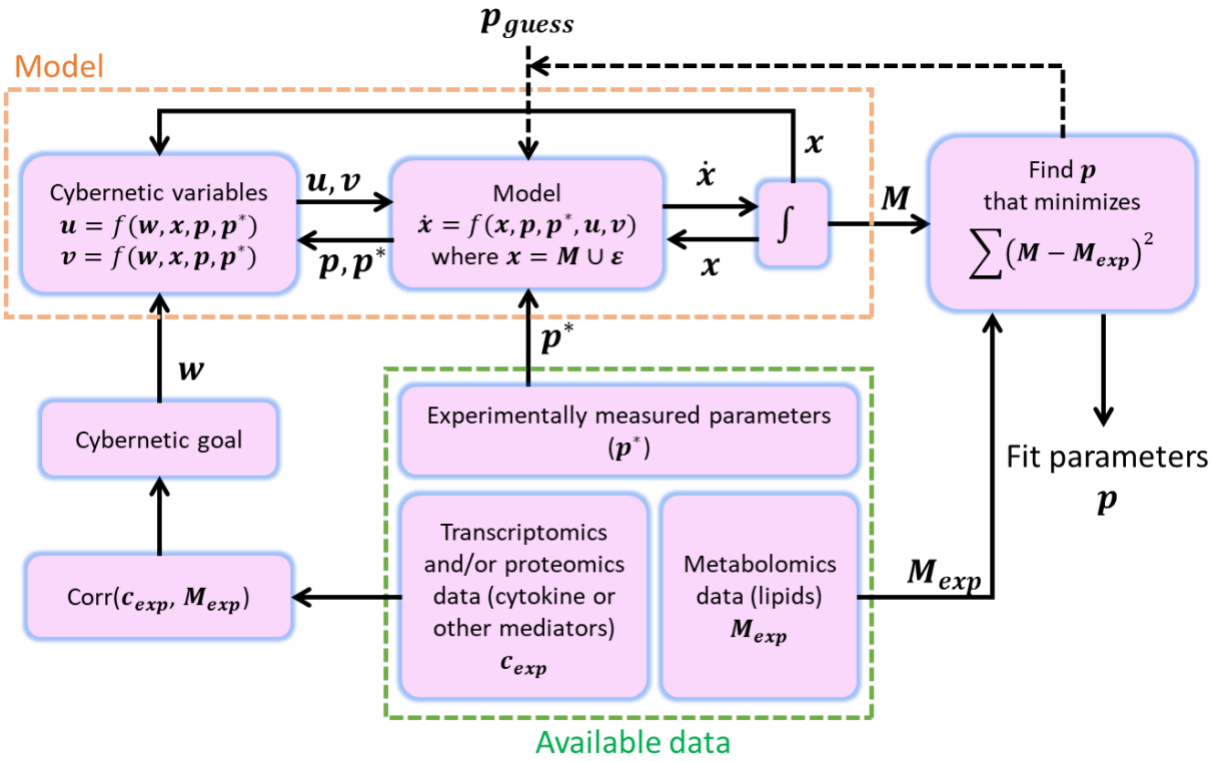

Figure 4.1. A schematic representing cybernetic modeling and determination of unknown parameters (***p***) (based on Aboulmouna et al. [32]). The cybernetic model is formulated using standard kinetic equations with the addition of a regulatory framework implemented through the cybernetic control variables u and v, obtained from the matching and proportional laws, respectively. The variable v regulates enzyme activity while u regulates enzyme synthesis, and each is computed from the reaction fluxes at a given branch point. The dynamic model consisting of kinetic mass balance equations is solved numerically, and the sum of the squares of the error between the simulated metabolite concentrations (M) and experimentally measured concentrations (M_{exp}) is minimized to estimate p. In the case of a cybernetic objective incorporating weights (w), a correlation between the experimental transcriptomic/proteomic data (c_{exp}) corresponding to the designated cybernetic objective and metabolomics data (M_{exp}) is used to calculate w. The weights (w) modulate the cybernetic control variables u and v.

4.2.2.1 Linear representation of a single objective

In the AA metabolic network [32], the cybernetic objective was implemented at the PGH_2 branch point where PGH_2 was converted to downstream products PGD_2, PGE_2, and $PGF_{2\alpha}$. The cybernetic objective determined the flux distribution based on the contribution of each metabolite (w_i) towards the production of TNF-α and was captured in the form of the cybernetic control

variables, v_i and u_i. These are computed from the Proportional and Matching laws [12], respectively, as follows:

$$v_i = \frac{w_i r_i^{kin} \varepsilon_i}{\max\limits_{j=1,2,\ldots,n}\left(w_j r_j^{kin} \varepsilon_j\right)} \quad , \qquad u_i = \frac{w_i r_i^{kin} \varepsilon_i}{\sum_{j=1}^{n}\left(w_j r_j^{kin} \varepsilon_j\right)} \tag{4.7}$$

where w_i is the weight for the i^{th} metabolite associated with a specific cybernetic objective and implicitly accounts for regulation by unmodeled processes. The cybernetic objective is a function of experimentally measured components; consequently, any parameters related to the cybernetic objective function can be computed directly.

The weights (w_i) in Aboulmouna et al. were calculated directly from experimental data (left-bottom blocks in Figure 4.1) by assuming a linear relationship between the three prostaglandin products and the cytokine TNF-α levels (adapted from Aboulmouna et al. [33])

$$[\dot{TNFa}] = \sum_i w_i [\dot{PG}_i] \tag{4.8}$$

The weights quantitatively accounted for the functional relevance of the PG metabolites for production of TNF-α (Equation 4.8). Once the dynamic model is fully defined, it is solved numerically, and the sum of the squares of the error (SSE) between the simulated metabolite concentrations (M_i) and experimentally measured concentrations ($\boldsymbol{M_{exp,i}}$) is minimized to estimate p (top-right block in Figure 4.1) [33,34]. For large systems with many parameters and limited measurements, a common challenge is over-fitting. To account for the effect of number of parameters on SSE, approaches similar to Akaike information criterion [90] or Bayesian information criterion [91], such

as λN + SSE (where N is the number of parameters and λ is a positive scalar), may help compare among several models of the system [92].

4.2.2.2 Nonlinear relation of cybernetic objectives using information theory

Using biological understanding and intuition to identify correlations between the metabolites and modulators is not always feasible. A vast amount of omics data available have information about links between these metabolites and modulators hidden in plain sight. New-age models like information theory and neural networks on these data can help us to identify the cybernetic goal. Use of these new-age models would allow for the inclusion of combinations of multiple objectives subsumed into one objective function that can account for non-linearities. A key factor in the delegation of the cybernetic objective is in exploring not only linear contributions, but nonlinear relationships between cytokines and prostaglandins. Information theoretic approaches could allow for the inclusion of combinations of multiple objectives subsumed into a single cybernetic goal that can account for nonlinearities. We expect that linking of the cybernetic model with the techniques mentioned previously can more effectively capture the regulatory mechanisms.

Macrophages are known to be cytokine factories signifying inflammation. In our prior work, we chose tumor necrosis factor alpha (TNF-α) as representing the inflammatory response for the objective function to be maximized, i.e. the cybernetic goal [86]. To incorporate the data on TNF-α in the optimization of the cybernetic goal, we built a linear relationship between proteomic data on TNF-α and lipidomic data on PGs using a least square fit, which, in principle, is based on correlation. We showed that, for a selected cybernetic goal, our model captures the complex regulation of PG metabolism and provides a reliable predictive description of PG formation [86]. However, the model excludes the role of other cytokines as an inflammatory

response and also does not account for the nonlinear relationship between cytokines and PGs. Further, cybernetic approaches rely on optimizing regulatory mechanisms for a given goal, and the goal is set a priori in an arbitrary manner. Developing information theoretic approaches to identify and optimize system goals in combination with optimizing the reaction rate and regulatory parameters can aid in more clearly defining the objective. This can be done by taking combinations of multiple phenotypic objectives subsumed into one optimal cybernetic goal for an organism using the maximization of mutual information between the weighted time series metabolite data and weighted combinations of multiple time series transcriptomic data [93].

We can expand the goal of the system to include combinations of multiple objectives subsumed into one optimal goal for an organism. Maximizing the mutual information (MI) between weighted time series metabolite data and weighted combinations of time series cytokine transcriptomic data would allow the extraction of information on the overall system goal as follows:

$$\max_{w_i, w'_j} \left(I\left(\sum_i w_i m_i \ , \sum_j w'_j c_j \right) \right), \text{ where } \sum_i w_i = 1 \text{ and } \sum_j w'_j = 1 \qquad 4.9$$

where I(x,y) is the MI between two variables x and y, w_i is weight associated with each pathway's (m_i) contribution to the formation rate of the multi-objective goal and w'_j is the weight associated with contribution of each cytokine (c_j) to the multi-objective goal ($\sum_j w'_j c_j$). Similar to Equation 4.8, the ROI for each pathway is assumed to be the amount of the goal that each unregulated pathway (associated w_i) can yield at each instant in time, which is described by ρ_i.

$$\rho_i = w_i r^{kin}_{m_a \to m_i} \qquad 4.10$$

MI between the weighted time-course vectors of metabolite levels and weighted time-course vectors of the cytokine levels can be optimized using efficient algorithms. In this case, due to the difference in magnitude of the different metabolite levels, a scaling of the metabolite levels will need to be carried out prior to correlating with the cytokines. Once the cybernetic goal of the system from maximizing the MI is obtained, the associated w_i can be used to optimize the parameters of the model using a two-step hybrid optimization procedure which involves application of effective global search techniques followed by a local deterministic search. Similar to the work in Chapter 3.2.4, the model can be parameterized and validated using existing data.

4.2.3 Quantify objective validity and determine overall system objective function

Cybernetic models have their origin in the hypothesis that metabolic regulation has evolved so that cells make optimal decisions when presented with metabolic choices [94]. The evolutionary history of an organism implies cellular objectives that change with time and environmental factors; determining well defined objective functions is the challenge, especially in the context of multicellular organisms.

The cybernetic approach differs substantially from other modeling methods. For traditional kinetic modeling, detailed metabolic regulatory mechanisms are necessary [67, 68]; however, the cybernetic approach models these regulatory actions as a collective process with an optimal system objective. Cybernetic enzymes and variables are used to describe a succinct mode of regulation related to the organism's goal. While we showed (Chapters 2 and 3) that cybernetic modeling predicts complex cellular phenomena, we also validated the assumption that the cybernetic control mechanisms mimic cellular regulation [66]. The cybernetic variables for enzyme synthesis and activity, u_i and v_i, were compared with cellular data that is representative of the regulatory mechanisms in cells. We showed that the scaled predicted enzyme profiles generally match the

behavior or trends of their corresponding genes identified from literature (Chapters 2.4.3 and 3.4.1). These predicted enzyme levels are calculated from metabolomics data and are made on the assumption that enzymes for substrate pathways are regulated in such a way as to optimize the objective function— formation of TNF-α. The predicted enzyme levels as informed by the e_i control variables are independent of the gene expression data. Qualitatively comparing the behavior of the dynamic gene expression profiles with the predicted enzyme levels further validated our cybernetic model (Figure 2.5) and served to validate the idea that modeling macrophage cells from a goal-oriented perspective is useful.

The objective function used in the model, e.g., maximizing the rate of TNF-α formation, is a central postulate of the cybernetic model presented here. While TNF-α is well characterized as a signaling molecule generated in the macrophage response of LPS binding to the TLR4 receptor, other inflammatory cytokines such as the interleukins (ILs) like IL-1, IL-6, and IL-12 can also be used to describe the goal of the system [95]. Control goals related to other functions of PGs besides inflammation are also of interest; however, given that the response of macrophages to ATP and KLA is an inflammatory one, the objective function centered around TNF-α seemed most relevant within the context of the system and conditions studied in Chapter 2. However, it is unclear if the proposed objective function's associated weights (w_i) are unique as seen in Chapter 3 when exploring multiple objectives and their validity in describing the system. As a result, it is critical to establish an approach that allows for a quantitative understanding of the relation between cybernetic variables and the cellular regulatory components as described by gene expression data.

4.3 Beyond the macrophage cell

Upon resolution of inflammation, the system's objectives may change. For instance, metabolic fluxes may be better indicated by pro- or anti-inflammatory cytokines depending on the

state of the macrophages [96-100]. Since there is dynamic remodeling between pro- and anti-inflammatory macrophage populations (M1 and M2, respectively) [101, 102], the correlation of events at different timescales can be highly dependent on distinct objectives. In order to model such a process, a list of mediators corresponding to multiple objectives supporting the different cellular functions is necessary. Using biological understanding and intuition to identify links between the metabolites and regulators is not always feasible; however, omics data (i.e., metabolomic and transcriptomic data) may facilitate identification of the correlations and potential links between these metabolites and regulators. While the current cybernetic model uses linear correlation to relate omics data, an alternate model can be proposed to estimate these cybernetic weights based on information theory approaches or by training a neural network [103, 104].

4.3.1 Macrophage cell polarization

An essential part of the inflammatory response is the resolution phase after the initial pro-inflammatory phase. The inflammation process is mediated by the production of multiple cytokines, chemokines, lipid mediators, etc. The early mediators are pro-inflammatory, whereas, the late mediators are anti-inflammatory or pro-resolution. These mediators could alter the cellular regulation of macrophages by receptor binding, thus creating positive and negative feedback loops. Inflammation, though a necessary process, if uncontrolled, could lead to chronic inflammation and several auto-immune diseases [66,67]. The negative regulation in the inflammatory cascade plays a vital role in the prevention of disease progression [40,68–71]. These mediators can alter the different subprocesses in inflammation.

One way to prevent uncontrolled inflammation is to polarize the macrophages to be anti-inflammatory [72]. Macrophages are divided into two cell types *in vitro* based on the type of stimulation: M1 (classically activated) associated with highly microbicidal and pro-inflammatory

responses that are stimulated by LPS and IFN-γ, and M2 (alternatively activated) associated with anti-inflammatory responses, tissue remodeling, and resolution of inflammation that are stimulated by anti-inflammatory stimuli like IL-4 [36,73]. Another classification provides three sub-types in M2 cells based on the stimulation [74]. But in vivo, transcriptome studies proposed a spectrum of macrophage activation states beyond that of M1/M2 dichotomy [75]. Modeling of macrophage cells can incorporate the presence of these cell groups. Their transition from one type to another may depend on mediators [76–78]. Each of these cell types have different metabolic regulation performing different function. Further, the production of these mediators could be affected by metabolism. Cybernetic regulation can be thus incorporated at the intracellular metabolic pathway and cellular level, creating a multi-level cybernetic formulation.

4.3.2 Use as a pharmaceutical model

COX inhibitors (nonsteroidal anti-inflammatory drugs (NSAIDs)) are common and found in daily-use drugs such as aspirin and ibuprofen [105]. Two isoforms of COX have been identified. COX-1 is expressed constitutively while COX-2 is an inducible enzyme. The two isoforms have diverse physiological and pathophysiological roles due to their structural differences and corresponding inhibitory profiles. Traditional NSAIDs block both COX-2 and COX-1 which consequently interfere with homeostatic function which includes blocking platelet activation. Both COX-1 and COX-2 share similar structural properties, including a hydrophobic region that allows AA access to the respective active sites. In COX-2, this hydrophobic region has an exposed side pocket which allows for COX-2 to have greater substrate recognition than COX-1. This structural difference in the active site of COX-2 has allowed for selective inhibition of COX-2 by compounds developed and marketed as anti-inflammatory drugs [106]. These drugs were known for their limited gastric toxicity to have an advantage over traditional NSAIDs [107, 108].

The magnitude and duration of the inflammatory response is regulated via a number of checkpoints. Defects in endogenous anti-inflammatory pathways predispose the host to chronic inflammatory diseases. An ideal approach to address this chronic inflammatory response would be in the development of therapeutics that exert multiple effects at various phases rather than suppressing the response in its entirety. In order to do this, it is crucial we develop a clearer understanding of the driving forces associated with each individual inflammatory response and tailor treatments accordingly. Additionally, it is necessary to better define the inflammatory response in order to determine ways in which we can enhance this process in conjunction with anti-inflammatory therapies.

Fatty acids (FAs) are simple lipids comprised of a carbon chain and a terminal carboxylic acid. Saturated FAs have no double bonds and are synthesized by chain elongation. Humans lack desaturases which modify single bonds to a double bond in FAs in the position distal to the $\Delta 9$ carbon. Consequently, it is required that we supplement our diets with essential FAs (EFAs). EFAs are further elongated and desaturated in our body resulting in ω3 and ω6 polyunsaturated fatty acids (PUFAs). Arachidonic acid is a representative ω6 PUFA and is a precursor of PGs, leukotrienes (LTs), and other oxygenated metabolites [109, 110]. As discussed in Chapter 1, inhibition of COX is a primary objective of many pharmaceutical initiatives. An expanded network model will allow us to understand how the inhibition of COX impacts downstream production of PGs in our network model. A prior study by Gupta et al. involves the competitive metabolism of AA and eicosapentaenoic acid (EPA) which acts in a similar mechanism to a COX inhibitor (Figure 3.2) in the eicosanoid metabolism network [51]. The ω3-PUFAs, such as EPA and docosahexaenoic acid (DHA), are now widely used as a supplement for health benefits. We will use the parameter set obtained from the KLA stimulated study to predict the response of EPA and

DHA on the metabolism of AA. This study represents an example of drug inhibition of COX using EPA as well as DHA [111].

4.4 Extension of cybernetics to other complex mammalian processes

The framework developed in Chapter 4.2 can be applied to several biochemical pathways. Our primary test example has been the macrophage system, where we have deep experimental knowledge of multiple outcome variables. Information theoretic cybernetic framework could identify the combination of cytokines, e.g., TNF-α, interleukins (ILs) IL-1, IL-6, and IL-12 to determine the optimal objective function [112]. Depending upon the system and conditions being modeled, one may need to incorporate more reactions and regulatory connections possibly spanning multiple timescales and involving multiple compartments. We provide some exemplar cases in the following.

NF-κB is a transcription factor, which is the critical mediator for cellular responses to a number of physiological responses such as inflammatory cytokines, developmental signals, and cellular stressors. NF-κB activity is inhibited by associating with IκB isoforms IκBα, IκBβ, IκBϵ, and IκBδ whose degradation and synthesis heavily regulate NF-κB signaling [113]. In this model, NF-κB will take on a similar role as the cytokines in the cybernetic goal and the IκB isoforms will serve a function similar to the metabolites described (Equation 4.9). The NF-κB network is regulated by two pathways: the canonical NF-κB essential modulator (NEMO)-dependent pathway and noncanonical NEMO-independent pathway. A transient TNF stimulus applied to the system to elucidate the functional significance of IκB degradation on NF-κB signaling via the canonical pathway could be modeled. Additionally, simulated model knock-down studies of individual IκB isomers will inform the role of NF-κB in regulating its own homeostasis [113].

Another example, involving the differentiation of multipotent thymic precursor cells into T-cells or myeloid cells, depends on the competition between PU.1 and Notch signals. Presence of PU.1 differentiates the precursor cells into myeloid cells. However, when Notch is present, precursor cells differentiate into T-cells [114]. In this case, we can dynamically optimize the T-cell or myeloid cell potential (markers) as the cybernetic goal/cell fate decision in relation to some function of PU.1 and Notch signaling. The results can then be validated with available flow cytometry data [114]. These examples highlight a limited application of cybernetics in immune related responses, but the cybernetic framework can be applied in any system where a well-defined cybernetic objective is identified.

4.5 Concluding remarks

The complexity of regulatory mechanisms in biological processes makes its explicit modeling difficult. The strength of cybernetics is in the ability to indirectly model this complexity using specific "goals". This powerful technique can capture non-linearities in biological systems without adding any additional parameters to simple enzymatic models. The approach is flexible and allows for the introduction of multiple objectives to describe complex behavior. In solving inverse problems in biological systems, as in our case, the collective behavior (overall phenotype) is much easier to measure than the individual parameters. The parameters are mostly unknown and experimental data can be noisy. Complete identifiability analysis can provide an estimate of the range of parameter values consistent with experimental data [115]. Another limitation while modeling complex systems is that the exact quantitative goal of the system is unknown—only a qualitative expectation is known. One can attempt to formulate a cybernetic goal based on multiple components or phenotypes (multiple-objectives) and the resulting optimization problem can be solved using the notion of pareto-optimality [116].

Cybernetic models have evolved over the years and have been used to model biological processes in several bacterial and yeast systems. For biological processes in mammalian systems, this thesis work establishes a framework for cybernetic modeling in these systems. However, cybernetic modeling in multicellular organisms is still in a nascent state but is yielding promising results [86, 117]. In multi-cellular organisms, temporal- and context-dependence of the "goal" can suggest the use of multiple objectives. Approaches based on the notion of pareto-optimality have a great potential to handle multiple objectives and will likely play an important role towards successful use of cybernetic modeling for mammalian systems.

The advantage to using cybernetic modeling is in its ability to capture system behavior without the same level of detail required for these interactions as typical kinetic modeling. However, the evolutionary history of an organism implies cellular objectives that change with time and environmental factors; determining well defined objective functions is the challenge, especially in the context of multicellular organisms. We have laid the groundwork for application of cybernetic modeling in complex mammalian systems. Insight into the metabolic goals of multicellular systems allows for a more complete understanding of how the states of these cells evolve over time. This insight can provide us the necessary knowledge to develop a greater understanding of dysregulation of the immune response and in the development of therapeutics for inflammatory diseases.

REFERENCES

1. Maurya, M.R. and S. Subramaniam, *Computational Challenges in Systems Biology.* Systems Biomedicine: Concepts and Perspectives, 2010: p. 177-223.

2. Gupta, S., et al., *Omics Approaches to Macrophage Biology.* Macrophages: Biology and Role in the Pathology of Diseases, 2014: p. 587-615.

3. DeRisi, J.L., V.R. Iyer, and P.O. Brown, *Exploring the metabolic and genetic control of gene expression on a genomic scale.* Science, 1997. **278**(5338): p. 680-6.

4. Rizzi, M., et al., *In vivo analysis of metabolic dynamics in Saccharomyces cerevisiae: II. Mathematical model.* Biotechnol Bioeng, 1997. **55**(4): p. 592-608.

5. Chassagnole, C., et al., *Dynamic modeling of the central carbon metabolism of Escherichia coli.* Biotechnol Bioeng, 2002. **79**(1): p. 53-73.

6. Zangirolami, T.C., et al., *Simulation of penicillin production in fed-batch cultivations using a morphologically structured model.* Biotechnol Bioeng, 1997. **56**(6): p. 593-604.

7. Hatzimanikatis, V., C.A. Floudas, and J.E. Bailey, *Optimization of regulatory architectures in metabolic reaction networks.* Biotechnol Bioeng, 1996. **52**(4): p. 485-500.

8. Jamshidi, N., et al., *Dynamic simulation of the human red blood cell metabolic network.* Bioinformatics, 2001. **17**(3): p. 286-7.

9. Morgan, J.A. and D. Rhodes, *Mathematical modeling of plant metabolic pathways.* Metab Eng, 2002. **4**(1): p. 80-9.

10. Orth, J.D., I. Thiele, and B.O. Palsson, *What is flux balance analysis?* Nat Biotechnol, 2010. **28**(3): p. 245-8.

11. Ramkrishna, D., *A Cybernetic Perspective of Microbial Growth*, in *Foundations of Biochemical Engineering: Kinetics and thermodynamics in biological systems*. 1982, American Chemical Society. p. 161-178.

12. Ramkrishna, D. and H.S. Song, *Cybernetic Modeling for Bioreaction Engineering*. Cambridge Series in Chemical Engineering. 2018, Cambridge: Cambridge University Press.

13. Dhurjati, P., et al., *A cybernetic view of microbial growth: modeling of cells as optimal strategists.* Biotechnol Bioeng, 1985. **27**(1): p. 1-9.

14. Kompala, D.S., et al., *Investigation of bacterial growth on mixed substrates: experimental evaluation of cybernetic models.* Biotechnol Bioeng, 1986. **28**(7): p. 1044-55.

15. Ramakrishna, R., D. Ramkrishna, and A.E. Konopka, *Cybernetic modeling of growth in mixed, substitutable substrate environments: Preferential and simultaneous utilization.* Biotechnol Bioeng, 1996. **52**(1): p. 141-51.

16. Song, H.S., et al., *Dynamic modeling of aerobic growth of Shewanella oneidensis. Predicting triauxic growth, flux distributions, and energy requirement for growth.* Metab Eng, 2013. **15**: p. 25-33.

17. Song, H.S. and D. Ramkrishna, *Prediction of dynamic behavior of mutant strains from limited wild-type data.* Metab Eng, 2012. **14**(2): p. 69-80.

18. Kim, J.I., et al., *Exacting predictions by cybernetic model confirmed experimentally: steady state multiplicity in the chemostat.* Biotechnol Prog, 2012. **28**(5): p. 1160-6.

19. Straight, J.V. and D. Ramkrishna, *Cybernetic Modeling and Regulation of Metabolic Pathways - Growth on Complementary Nutrients.* Biotechnology Progress, 1994. **10**(6): p. 574-587.

20. Varner, J.D., *Large-scale prediction of phenotype: concept.* Biotechnol Bioeng, 2000. **69**(6): p. 664-78.

21. Varner, J. and D. Ramkrishna, *Metabolic engineering from a cybernetic perspective: aspartate family of amino acids.* Metab Eng, 1999. **1**(1): p. 88-116.

22. Gadkar, K.G., et al., *Cybernetic model predictive control of a continuous bioreactor with cell recycle.* Biotechnol Prog, 2003. **19**(5): p. 1487-97.

23. Namjoshi, A.A. and D. Ramkrishna, *A cybernetic modeling framework for analysis of metabolic systems.* Computers & Chemical Engineering, 2005. **29**(3): p. 487-498.

24. Young, J.D. and D. Ramkrishna, *On the matching and proportional laws of cybernetic models.* Biotechnology Progress, 2007. **23**(1): p. 83-99.

25. Kim, J.I., J.D. Varner, and D. Ramkrishna, *A Hybrid Model of Anaerobic E. coli GJT001: Combination of Elementary Flux Modes and Cybernetic Variables.* Biotechnology Progress, 2008. **24**(5): p. 993-1006.

26. Schuster, S., D.A. Fell, and T. Dandekar, *A general definition of metabolic pathways useful for systematic organization and analysis of complex metabolic networks.* Nature Biotechnology, 2000. **18**(3): p. 326-332.

27. Wong, W.C., et al., *Hybrid cybernetic model-based simulation of continuous production of lignocellulosic ethanol: Rejecting abruptly changing feed conditions.* Control Engineering Practice, 2010. **18**(2): p. 177-189.

28. Song, H.S. and D. Ramkrishna, *Cybernetic models based on lumped elementary modes accurately predict strain-specific metabolic function.* Biotechnol Bioeng, 2011. **108**(1): p. 127-40.

29. Song, H.S. and D. Ramkrishna, *Prediction of Metabolic Function From Limited Data: Lumped Hybrid Cybernetic Modeling (L-HCM).* Biotechnology and Bioengineering, 2010. **106**(2): p. 271-284.

30. Turner, B.G., D. Ramkrishna, and N.B. Jansen, *Cybernetic modeling of bacterial cultures at low growth rates: Mixed-substrate systems.* Biotechnol Bioeng, 1988. **32**(1): p. 46-54.

31. Young, J.D., et al., *Integrating cybernetic modeling with pathway analysis provides a dynamic, systems-level description of metabolic control.* Biotechnol Bioeng, 2008. **100**(3): p. 542-59.

32. Koh, T.J. and L.A. DiPietro, *Inflammation and wound healing: the role of the macrophage.* Expert Rev Mol Med, 2011. **13**: p. e23.

33. Wang, Q., G. Hasan, and C.W. Pikielny, *Preferential expression of biotransformation enzymes in the olfactory organs of Drosophila melanogaster, the antennae.* J Biol Chem, 1999. **274**(15): p. 10309-15.

34. Lien, E., et al., *Toll-like receptor 4 imparts ligand-specific recognition of bacterial lipopolysaccharide.* J Clin Invest, 2000. **105**(4): p. 497-504.

35. Kawasaki, K., et al., *Mouse toll-like receptor 4 center dot MD-2 complex mediates lipopolysaccharide-mimetic signal transduction by taxol.* Journal of Biological Chemistry, 2000. **275**(4): p. 2251-2254.

36. Poltorak, A., et al., *Physical contact between lipopolysaccharide and Toll-like receptor 4 revealed by genetic complementation.* Proceedings of the National Academy of Sciences of the United States of America, 2000. **97**(5): p. 2163-2167.

37. Schromm, A.B., et al., *Molecular genetic analysis of an endotoxin nonresponder mutant cell Line: A point mutation in a conserved region of MD-2 abolishes endotoxin-induced signaling.* Journal of Experimental Medicine, 2001. **194**(1): p. 79-88.

38. Shimazu, R., et al., *MD-2, a molecule that confers lipopolysaccharide responsiveness on Toll-like receptor 4.* Journal of Experimental Medicine, 1999. **189**(11): p. 1777-1782.

39. Yang, R.B., et al., *Toll-like receptor-2 mediates lipopolysaccharide-induced cellular signalling.* Nature, 1998. **395**(6699): p. 284-288.

40. Correia, J.D., et al., *Lipopolysaccharide is in close proximity to each of the proteins in its membrane receptor complex - Transfer from CD14 to TLR4 and MD-2.* Journal of Biological Chemistry, 2001. **276**(24): p. 21129-21135.

41. Di Virgilio, F., *Purinergic signalling in the immune system. A brief update.* Purinergic Signal, 2007. **3**(1-2): p. 1-3.

42. Junger, W.G., *Immune cell regulation by autocrine purinergic signalling.* Nat Rev Immunol, 2011. **11**(3): p. 201-12.

43. Jarvis, M.F. and B.S. Khakh, *ATP-gated P2X cation-channels.* Neuropharmacology, 2009. **56**(1): p. 208-15.

44. Remmerie, A. and C.L. Scott, *Macrophages and lipid metabolism.* Cell Immunol, 2018.

45. Hubler, M.J. and A.J. Kennedy, *Role of lipids in the metabolism and activation of immune cells.* J Nutr Biochem, 2016. **34**: p. 1-7.

46. Fahy, E., et al., *Update of the LIPID MAPS comprehensive classification system for lipids.* J Lipid Res, 2009. **50 Suppl**: p. S9-14.

47. Funk, C.D., *Prostaglandins and leukotrienes: advances in eicosanoid biology.* Science, 2001. **294**(5548): p. 1871-5.

48. Shimizu, T., *Lipid mediators in health and disease: enzymes and receptors as therapeutic targets for the regulation of immunity and inflammation.* Annu Rev Pharmacol Toxicol, 2009. **49**: p. 123-50.

49. Gupta, S., et al., *An integrated model of eicosanoid metabolism and signaling based on lipidomics flux analysis.* Biophys J, 2009. **96**(11): p. 4542-51.

50. Kihara, Y., et al., *Modeling of eicosanoid fluxes reveals functional coupling between cyclooxygenases and terminal synthases.* Biophys J, 2014. **106**(4): p. 966-75.

51. Gupta, S., et al., *Computational Modeling of Competitive Metabolism between omega3- and omega6-Polyunsaturated Fatty Acids in Inflammatory Macrophages.* J Phys Chem B, 2016. **120**(33): p. 8346-53.

52. Gupta, S., et al., *Integration of lipidomics and transcriptomics data towards a systems biology model of sphingolipid metabolism.* BMC Syst Biol, 2011. **5**: p. 26.

53. Suzuki, T., et al., *Production and release of neuroprotective tumor necrosis factor by P2X7 receptor-activated microglia.* J Neurosci, 2004. **24**(1): p. 1-7.

54. van der Bruggen, T., et al., *Lipopolysaccharide-induced tumor necrosis factor alpha production by human monocytes involves the raf-1/MEK1-MEK2/ERK1-ERK2 pathway.* Infect Immun, 1999. **67**(8): p. 3824-9.

55. Kanehisa, M., et al., *KEGG as a reference resource for gene and protein annotation.* Nucleic Acids Res, 2016. **44**(D1): p. D457-62.

56. Tanabe, M. and M. Kanehisa, *Using the KEGG database resource.* Curr Protoc Bioinformatics, 2012. **Chapter 1**: p. Unit1 12.

57. Sud, M., et al., *LMSD: LIPID MAPS structure database.* Nucleic Acids Res, 2007. **35**(Database issue): p. D527-32.

58. Ogata, H., et al., *KEGG: Kyoto Encyclopedia of Genes and Genomes.* Nucleic Acids Res, 1999. **27**(1): p. 29-34.

59. Remmerie, A. and C.L. Scott, *Macrophages and lipid metabolism.* Cell Immunol, 2018. **330**: p. 27-42.

60. Zhang, J.M. and J. An, *Cytokines, inflammation, and pain.* Int Anesthesiol Clin, 2007. **45**(2): p. 27-37.

61. Hanna, V.S. and E.A.A. Hafez, *Synopsis of arachidonic acid metabolism: A review.* Journal of Advanced Research, 2018. **11**: p. 23-32.

62. Dennis, E.A., et al., *A mouse macrophage lipidome.* J Biol Chem, 2010. **285**(51): p. 39976-85.

63. Dinasarapu, A.R., et al., *A combined omics study on activated macrophages--enhanced role of STATs in apoptosis, immunity and lipid metabolism.* Bioinformatics, 2013. **29**(21): p. 2735-43.

64. Subramaniam, S., et al., *Bioinformatics and systems biology of the lipidome.* Chem Rev, 2011. **111**(10): p. 6452-90.

65. DeVilbiss, F.T., *Is metabolism goal-directed? Investigating the validaty of modeling biological systems with cybernetic control via omic data*, in *Chemical Engineering*2016, Purdue University: Open Access Dissertations.

66. DeVilbiss, F., A. Mandli, and D. Ramkrishna, *Consistency of cybernetic variables with gene expression profiles: A more rigorous test.* Biotechnol Prog, 2018.

67. Jahan, N., et al., *Development of an accurate kinetic model for the central carbon metabolism of Escherichia coli.* Microb Cell Fact, 2016. **15**(1): p. 112.

68. Kotte, O., J.B. Zaugg, and M. Heinemann, *Bacterial adaptation through distributed sensing of metabolic fluxes.* Mol Syst Biol, 2010. **6**: p. 355.

69. Boulet, L., et al., *Deletion of microsomal prostaglandin E2 (PGE2) synthase-1 reduces inducible and basal PGE2 production and alters the gastric prostanoid profile.* J Biol Chem, 2004. **279**(22): p. 23229-37.

70. Schomburg, I., et al., *BRENDA, the enzyme database: updates and major new developments.* Nucleic Acids Res, 2004. **32**(Database issue): p. D431-3.

71. Lazarus, M., et al., *Biochemical characterization of mouse microsomal prostaglandin E synthase-1 and its colocalization with cyclooxygenase-2 in peritoneal macrophages.* Arch Biochem Biophys, 2002. **397**(2): p. 336-41.

72. Tanioka, T., et al., *Molecular identification of cytosolic prostaglandin E2 synthase that is functionally coupled with cyclooxygenase-1 in immediate prostaglandin E2 biosynthesis.* J Biol Chem, 2000. **275**(42): p. 32775-82.

73. Chan, G., et al., *Cyclooxygenase-2 expression is up-regulated in squamous cell carcinoma of the head and neck.* Cancer Res, 1999. **59**(5): p. 991-4.

74. Urade, Y., et al., *Mast cells contain spleen-type prostaglandin D synthetase.* J Biol Chem, 1990. **265**(1): p. 371-5.

75. Shimizu, T., S. Yamamoto, and O. Hayaishi, *Purification and properties of prostaglandin D synthetase from rat brain.* J Biol Chem, 1979. **254**(12): p. 5222-8.

76. Dennis, E.A., et al., *A Mouse Macrophage Lipidome.* Journal of Biological Chemistry, 2010. **285**(51): p. 39976-39985.

77. Fahy, E., et al., *Update of the LIPID MAPS comprehensive classification system for lipids.* Journal of Lipid Research, 2009. **50**(SUPPL.): p. 9-14.

78. Hubler, M.J. and A.J. Kennedy, *Role of lipids in the metabolism and activation of immune cells.* Journal of Nutritional Biochemistry, 2016. **34**: p. 1-7.

79. Remmerie, A. and C.L. Scott, *Macrophages and lipid metabolism.* Cellular Immunology, 2018. **330**(February): p. 27-42.

80. Dennis, E.A. and P.C. Norris, *Eicosanoid storm in infection and inflammation.* Nature Reviews Immunology, 2015. **15**(8): p. 511-523.

81. Gupta, S., et al., *Integration of lipidomics and transcriptomics data towards a systems biology model of sphingolipid metabolism.* Bmc Systems Biology, 2011. **5**.

82. Ricciotti, E. and G.A. FitzGerald, *Prostaglandins and Inflammation.* Arteriosclerosis Thrombosis and Vascular Biology, 2011. **31**(5): p. 986-1000.

83. Fitzpatrick, F.A., *Cyclooxygenase enzymes: Regulation and function.* Current Pharmaceutical Design, 2004. **10**(6): p. 577-588.

84. Gupta, S., et al., *An integrated model of eicosanoid metabolism and signaling based on lipidomics flux analysis.* Biophysical Journal, 2009. **96**(11): p. 4542-4551.

85. Kihara, Y., et al., *Modeling of eicosanoid fluxes reveals functional coupling between cyclooxygenases and terminal synthases.* Biophysical Journal, 2014. **106**(4): p. 966-975.

86. Aboulmouna, L., et al., *A cybernetic approach to modeling lipid metabolism in mammalian cells.* Processes, 2018. **6**(8).

87. Falvo, J.V., A.V. Tsytsykova, and A.E. Goldfeld, *Transcriptional Control of the TNF Gene.* Tnf Pathophysiology: Molecular and Cellular Mechanisms, 2010. **11**: p. 27-60.

88. Peters-Golden, M. and W.R. Henderson, *Mechanisms of disease: Leukotrienes.* New England Journal of Medicine, 2007. **357**(18): p. 1841-1854.

89. Ramkrishna, D., *A Cybernetic Perspective of Microbial Growth*, in *Foundations of Biochemical Engineering: Kinetics and Thermodynamics in Biological Systems*, E.T.P. Harvey W. Blanch, Gregory Stephanopoulos, Editor. 1983, American Chemical Society. p. 161-178.

90. Stone, M., *An Asymptotic Equivalence of Choice of Model by Cross-Validation and Akaike's Criterion.* Journal of the Royal Statistical Society. Series B, Methodological, 1977. **39**(1): p. 44-47.

91. Schwarz, G.E., *Estimating the dimension of a model.* Annals of Statistics, 1986. **14**(2): p. 590-606.

92. Devilbiss, F. and D. Ramkrishna, *Addressing the Need for a Model Selection Framework in Systems Biology Using Information Theory.* Proceedings of the IEEE, 2017. **105**(2): p. 330-339.

93. Farhangmehr, F., et al., *Information theoretic approach to complex biological network reconstruction: application to cytokine release in RAW 264.7 macrophages.* Bmc Systems Biology, 2014. **8**.

94. Ramkrishna, D., *A Cybernetic Perspective of Microbial-Growth.* Acs Symposium Series, 1983. **207**: p. 161-178.

95. Balkwill, F.R. and F. Burke, *The cytokine network.* Immunol Today, 1989. **10**(9): p. 299-304.

96. Buckley, C.D., D.W. Gilroy, and C.N. Serhan, *Proresolving Lipid Mediators and Mechanisms in the Resolution of Acute Inflammation.* Immunity, 2014. **40**(3): p. 315-327.

97. Hamidzadeh, K., et al., *Macrophages and the Recovery from Acute and Chronic Inflammation.* Annual Review of Physiology, Vol 79, 2017. **79**: p. 567-592.

98. Harris, S.G., et al., *Prostaglandins as modulators of immunity.* Trends in Immunology, 2002. **23**(3): p. 144-150.

99. Kong, D.P., et al., *PKA regulatory II alpha subunit is essential for PGD(2)-mediated resolution of inflammation.* Journal of Experimental Medicine, 2016. **213**(10): p. 2209-2226.

100. Scher, J.U. and M.H. Pillinger, *The Anti-Inflammatory Effects of Prostaglandins.* Journal of Investigative Medicine, 2009. **57**(6): p. 703-708.

101. Diskin, C. and E.M. Palsson-McDermott, *Metabolic Modulation in Macrophage effector Function.* Frontiers in Immunology, 2018. **9**.

102. Thapa, B. and K. Lee, *Metabolic influence on macrophage polarization and pathogenesis.* Bmb Reports, 2019. **52**(6): p. 360-372.

103. Farhangmehr, F., et al., *Information theoretic approach to complex biological network reconstruction: Application to cytokine release in RAW 264.7 macrophages.* BMC Systems Biology, 2014. **8**(1): p. 1-16.

104. Nakaya, H.I., et al., *Systems Analysis of Immunity to Influenza Vaccination across Multiple Years and in Diverse Populations Reveals Shared Molecular Signatures.* Immunity, 2015. **43**(6): p. 1186-1198.

105. Smith, W.L., D.L. DeWitt, and R.M. Garavito, *Cyclooxygenases: structural, cellular, and molecular biology.* Annu Rev Biochem, 2000. **69**: p. 145-82.

106. Kurumbail, R.G., et al., *Structural basis for selective inhibition of cyclooxygenase-2 by anti-inflammatory agents.* Nature, 1996. **384**(6610): p. 644-648.

107. Bombardier, C., et al., *Comparison of upper gastrointestinal toxicity of rofecoxib and naproxen in patients with rheumatoid arthritis. VIGOR Study Group.* N Engl J Med, 2000. **343**(21): p. 1520-8, 2 p following 1528.

108. Silverstein, F.E., et al., *Gastrointestinal toxicity with celecoxib vs nonsteroidal anti-inflammatory drugs for osteoarthritis and rheumatoid arthritis: the CLASS study: A randomized controlled trial. Celecoxib Long-term Arthritis Safety Study.* JAMA, 2000. **284**(10): p. 1247-55.

109. Buczynski, M.W., D.S. Dumlao, and E.A. Dennis, *Thematic Review Series: Proteomics. An integrated omics analysis of eicosanoid biology.* J Lipid Res, 2009. **50**(6): p. 1015-38.

110. Quehenberger, O. and E.A. Dennis, *The human plasma lipidome.* N Engl J Med, 2011. **365**(19): p. 1812-23.

111. Wada, M., et al., *Enzymes and receptors of prostaglandin pathways with arachidonic acid-derived versus eicosapentaenoic acid-derived substrates and products.* J Biol Chem, 2007. **282**(31): p. 22254-66.

112. Balkwill, F.R. and F. Burke, *The Cytokine Network.* Immunology Today, 1989. **10**(9): p. 299-303.

113. O'dea, E.L., et al., *A homeostatic model of I kappa B metabolism to control constitutive NF-kappa B activity.* Molecular Systems Biology, 2007. **3**.

114. Del Real, M.M. and E.V. Rothenberg, *Architecture of a lymphomyeloid developmental switch controlled by PU.1, Notch and Gata3.* Development, 2013. **140**(6): p. 1207-1219.

115. Guzzi, R., T. Colombo, and P. Paci, *Inverse Problems in Systems Biology: A Critical Review.* Methods Mol Biol, 2018(1702): p. 25.

116. Belure, S., O. Shir, and V. Nanda, *Reaching the Pareto frontier in multi-objective protein design.* European Biophysics Journal with Biophysics Letters, 2017. **46**: p. S81-S81.

117. Martínez, J.A., et al., *Dynamic Modeling of CHO Cell Metabolism Using the Hybrid Cybernetic Approach With a Novel Elementary Mode Analysis Strategy.* 2020. **8**(April): p. 1-23.